The role of late Quaternary tectonic activity and sea-level changes on sedimentary processes interaction in the Gulf of Cadiz upper and middle continental slope (SW Iberia)

García, M.[1,2,*], Llave, E.[3], Hernández-Molina, F.J.[4], Lobo, F.J.[2], Ercilla, G.[5], Alonso, B.[5], Casas, D.[5], Mena, A.[6], Fernández-Salas, L.M.[1].

[1] Spanish Institute of Oceanography, Centre of Cadiz. Muelle Pesquero s/n, Cadiz. marga.garcia@ieo.es (*Corresponding author); luismi.fernandez@ieo.es
[2] Andalusian Institute of Earth Sciences, CSIC-UGR. Avda. de las Palmeras 4, Armilla (Granada). francisco.lobo@csic.es
[3] Spanish Geological Survey. C/ La Calera, 1, Tres Cantos (Madrid). e.llave@igme.es
[4] Department of Earth Sciences, Royal Holloway University of London. Egham Hill, Egham TW20 0EX, UK. Javier.Hernandez-Molina@rhul.ac.uk
[5] Institute of Marine Sciences, CSIC. Passeig Marítim de la Barceloneta, 37-49. Barcelona. gemma@icm.csic.es; belen@icm.csic.es; davidcasas@icm.csic.es
[6] Department of Marine Geosciences and Land Management, University of Vigo. CUVI, Vigo. anxomena@uvigo.es

Abstract

A morphological and seismic-stratigraphic analysis of the Gulf of Cadiz area near the Strait of Gibraltar is presented in this work, focused on the sedimentary evolution of the upper and proximal middle-continental slope since the Mid-Pleistocene. Based on the analysis of seismic reflection profiles and swath bathymetry data, this work analyses the close influence of the activity of buried and outcropping diapiric ridges and late Quaternary sea-level changes on the evolution of contouritic features related to the Mediterranean Outflow Water (MOW) and Eastern North Atlantic Central Water (ENACW), gravitational features and fluid-escape structures. The stratigraphic architecture reveals that, under active diapiric deformation, the upper slope plastered drift grew during low sea-level stages, when sediment supply was high and the ENACW swept the upper slope, contrasting with the present-day highstand situation dominated by northwest-trending MOW flow. The south-estward ENACW flow forced asymmetry and lateral migration of gullies incised in the plastered drift. Two evolutionary stages have been established: 1) After the Mid Pleistocene, activity of diapirs with a NE trend determined the location of the deepest depressions which were infilled by plastered contouritic drifts; 2) Between Late Quaternary and present, a drastic change of buried diapirs growth pattern and orientation to a NW trend enhanced slope-derived gravitational processes affecting the bottom current dynamics. Adjustments to tectonic changes led to a phase of plastered drift growth on the upper slope during which depocenters varied their distribution and orientation. In a long-term the structural control on sedimentation shows a northwestward displacement of deformation, resulting in an overall extension of the contourite depositional system to the NW. In a short-term, sea-level changes favoured drift deposition, gullies incision and the strengthening of water masses. This work evidences the importance of tectonic deformation in sedimentation at recent time scales, and the two-directional interplay between recent tectonic activity and bottom current dynamics.

Keywords: Tectonics; Sea-level; Diapirs; Contourites; Gullies; Seismic stratigraphy; Continental slope; Gulf of Cadiz.

1. Introduction

Sedimentary processes in siliciclastic continental margins are controlled by the interactions of regional basin tectonics, sea-level fluctuations and sediment supply (Haq et al., 1987; Richards et al., 1998). In fact, tectonism may in the long term control climate and sea-level (Mack, 1978). Under this ultimate control, numerous sedimentary processes interplay in shaping continental margins (Nelson and Maldonado, 1988; Viana, 2009; Shanmugan, 2012). A growing body of evidence indicates that interactions between downslope gravitational processes and alongslope oceanograpic processes are ubiquitous in numerous deep-water settings (Howe, 1996; Gong et al., 2013; Teixeira et al., 2019; and that they are of high importance in terms of hydrocarbon potential (Rodríguez and Hodgson, 2019). The interactions between turbidity flows and contour currents may be coeval (Mulder et al., 2008; Ercilla et al., 2019), forming hybrid (or mixed) depositional systems which are represented in the stratigraphic record as unidirectionally migrating turbiditic channels (Gong et al., 2013, 2018; Li et al., 2013), asymmetric turbiditic channels, laterally migrating levees (Carter and Carter, 1988; Michels et al., 2002; Kuvaas et al., 2004; Sansom, 2018; Serra et al., 2020) that may eventually evolve into mixed contourite drifts (Rebesco et al., 2002), and laterally elongated fans (Fonnesu et al., 2020). Regional conditions may also favour the co-existence of turbiditic fans and contouritic drifts (Locker and Laine, 1992; Michels et al., 2002; Ercilla et al., 2016; Juan et al., 2020). Another type of interaction is represented by turbidity systems reworked or even eroded by subsequent bottom current intensification (Locker and Laine, 1992; Mulder et al., 2009; Miramontes et al., 2019). In the opposite case, pre-existing contourite drifts may be dismantled by mass movements that evolve distally into turbiditic deposits (e.g., Martorelli et al., 2016; Teixeira et al., 2019). Finally, turbidites (or more generally, the products of mass flows) may alternate along time with contourites in the long term, where turbiditic products are progressively substituted by contourite drifts (Locker and Laine, 1992; Rasmussen et al., 2003), or driven by glacial-interglacial sea-level cyclicity, leading to high-frequency turbiditic-contouritic sequences (Mulder et al., 2009).

The Gulf of Cadiz hosts an extensive contourite depositional system, particularly documented along the Iberian margin, where the action of bottom currents over a complex, irregular seafloor topography has generated different morpho-sedimentary erosive and depositional sectors (Hernández-Molina et al., 2003, 2006; Llave et al., 2007a,b). Interactions between a number of gravity-driven and bottom current-related processes are common in the Gulf of Cadiz, such as: the development of gravitational erosive valleys that were later reoccupied by MOW filaments in the middle slope (Hanquiez et al.,

2010); long-term to short-term alternations between downslope mass wasting/turbidite systems and alongslope contourite systems (Brackenridge et al., 2013; Alonso et al., 2016; García et al., 2016); deviation of the main MOW flow by submarine canyons and differential development of contourite drifts (Mulder et al., 2006; Marchès et al., 2007) and high-frequency turbidite-contourite variability in a slope terrace located between two submarine canyons (Marchès et al., 2010) south of Portugal.

In the Gulf of Cadiz continental slope close to the Strait of Gibraltar, interactions between contouritic and gravity-driven processes have not been fully appreciated. However, this area is ideal for studying such kind of interactions, due to the occurrence of several outcropping and buried diapiric bodies and ridges (Fernández-Puga et al., 2007), and their associated tectonic deformation (León et al., 2010). The obstacle effect caused by the diapiric structures may influence bottom currents, generating a suite of contourite depositional and erosional morphologies such as contourite channels and sediment drifts (Palomino et al., 2016; Schattner et al., 2018). In addition, oversteepening due to halokinetic processes and their associated overburden and faulting may favour the occurrence of slope instabilities and associated mass movements (Cashman and Popenoe, 1985; Tripsanas et al., 2003, 2004; Akinci and Sawyer, 2016; Maselli and Kneller, 2018).

The interactions between the MOW and the middle slope erosive and depositional features have been extensively studied and increased effort is invested in investigating the present-day influence of the oceanographic dynamics with sedimentary processes at the seafloor (Lozano et al., 2020). However glacio-eustatic cyclicity has been demonstrated to induce important changes in the spatial distribution of water masses along glacial cycles (Llave et al., 2001, 2006, 2007a,b, Toucanne et al., 2007; Marchès et al., 2010; Roque et al., 2012), suggesting that present-day morphology may result from oceanographic patterns that were significantly different from the current ones. Considering the existing knowledge gaps in understanding the evolution of this part of the margin, this study aims to understand how the interactions between tectonic, sedimentary and oceanographic processes have controlled the evolution of the continental slope in the vicinity of the Strait of Gibraltar. For this purpose, the study area extends from the upper slope to the proximal middle slope of the northern Gulf of Cadiz to a maximum water depth of about 600 m (36º10'-36º40'N, 6º30'-7º'W). In particular, this work aims at investigating the interactions between the diapiric structures and their associated tectonic deformation and the climatically controlled gravitational and contouritic processes since the middle Pleistocene.

2. Geological and oceanographic framework

2.1. Geological setting

The Gulf of Cadiz is located at the Atlantic side of the Strait of Gibraltar, limited to the north by the SW Iberian Peninsula and to the south by NW Africa (Fig. 1a). The present-day geological setting is the result of a complex tectonic history, after the opening of the Neo-Tethys and Central Atlantic in the Triassic (Terrinha et al., 2002; Medialdea et al., 2009), and a series of tectonic phases related to the movements along the African-Eurasian plate boundary (Rosenbaum et al., 2002). Half-graben and horst structures produced by Mesozoic extension were reactivated as dextral strike slip faults during Cenozoic compressional events (Lopes et al., 2006). During the Burdigalian-Middle Tortonian, the westward drift of the Alboran Crustal Domain generated the Betic-Rifean thrust belt during a compressive phase that reactivated NNW-SSE to NW-SE structures (Rosenbaum et al., 2002; Platt et al., 2003, 2013). As a result, the Allochthonous Unit of the Gulf of Cadiz (AUGC) was emplaced during the Late Tortonian (Torelli et al., 1997; Maldonado et al., 1999; Somoza et al., 1999; Medialdea et al., 2004, 2009; Gütscher et al., 2009, 2012) and was reactivated in the Late Miocene to Present due to NW compression. Salt diapirism rooted in Triassic evaporites and Miocene clay and marl diapirism related to the AUGC (Medialdea et al., 2009) have produced widespread NE-SW-oriented diapiric ridges (Cadiz, Guadalquiver and Doñana diapiric ridges, Fig. 1) that have been reactivated during the Pliocene–Quaternary as the result of adjustments in the allochtonous unit under a dominant NW-SE compressive regime (García et al., 2009; Fernández-Puga et al., 2010; Hernandez-Molina et al., 2016). Major structures in the Gulf of Cadiz (thrust faults, strike-slip faults, extensional faults and diapirs) favour the upward fluid escape that originate minor features as mud volcanoes and pockmarks (Casas et al., 2003; Somoza et al., 2003; Fernández-Puga et al., 2007).

2.2. Oceanographic setting

The present-day oceanographic setting of the Gulf of Cadiz is dominated by the water exchange between the Mediterranean Sea and the Atlantic Ocean, through the Strait of Gibraltar (Figs. 1a and 2). At the western side of the strait, the water column along the Gulf of Cadiz continental margin is occupied by distinct water masses. The inner shelf waters reach depths down to 60 m, impinging directly on the continental shelf and are subject to coastal and atmospheric influence (Bellanco and Sánchez-Leal., 2016; Sánchez-Leal et al., 2017). The low-salinity Eastern North Atlantic Central Water (ENACW) circulates with the same direction but at depths of 100-250 m, affecting the outer continental shelf and the shallower upper slope. Below, the Mediterranean Outflow Water (MOW) circulates towards the NW (Fig. 2b; Sánchez-Leal et al., 2017) sweeping most of the upper slope and the middle slope. The MOW, after exiting the Strait of Gibraltar at depths deeper than 150-200 m veers towards the NW, where it is affected by the interaction with the rough topography (Fig. 2a; Sánchez-Leal et al., 2017). Its upper boundary deepens as it flows north-westwards along the Gulf of Cadiz continental margin and it is split into two preferential pathways forming the Mediterranean

Upper Core (MU), that flows along the base of the upper slope, and the Mediterranean Lower Core (ML), flowing along the middle slope (Fig. 1a; Madelain, 1970; Zenk, 1975; Grundlingh, 1981; Borenäs et al., 2002; Serra et al., 2005, 2010; Sánchez-Leal et al., 2017). The modified Antarctic Intermediate Water (AAIW) also flows towards the NW, down to depths of 600-625 m, and confines the MOW and the ENACW against the continental slope (Louarn and Morin, 2011; Hernandez-Molina et al., 2014; Roque et al., 2019). Finally, the North Atlantic Deep Water (NADW) flows below the MOW towards the E-SE at water depths >1500 m (Zenk, 1975; Thorpe, 1976; Gardner and Kidd, 1983; Ochoa and Bray, 1991; Baringer and Price, 1999; Serra et al., 2005).

The oceanographic pattern in the Gulf of Cadiz is highly dynamic and exhibits drastic seasonal changes. During the month of March,cooler and less saline waters (temperature of 14.6ºC and practical salinity of 36.26) occupy the inner shelf due to the erosion of the seasonal thermocline and the increase in river water supply and denser MOW (colder and more saline) invades the upper slope, displacing the ENACW towards the shelf. In November conditions, the water stratification is intensified and the ENACW broadens and stretches eastwards (Bellanco and Sánchez-Leal, 2016). In addition, a displacement of the MOW toward the upper continental slope is further favored by the increased presence of AAIW and a reduction of the ENACW (Roque et al., 2019).

2.3. The Gulf of Cadiz Contourite Depositional System

The Gulf of Cadiz hosts a huge contourite depositional system (CDS), created by the MOW as it exits the Strait of Gibraltar into the Atlantic Ocean. This system has been extensively studied in the last decades (Gonthier et al., 1984; Nelson et al., 1993, 1999; Maldonado et al., 1999; Llave et al., 2001, 2007; Hernández-Molina et al., 2003, 2016; Roque et al., 2012), mostly focusing on the erosional and depositional features in the middle slope (Fig. 1a; Hernández-Molina et al., 2006). The study area lies in the limit between the proximal scour and sand ribbons sector, close to the Strait of Gibraltar, and the active contourite drift sector towards the NW (1 and 2 respectively in Fig. 1a). The proximal sector presents two channel-terrace systems, Northern and Southern, that connect with the middle slope contourite channels (Hernández-Molina et al., 2014). The active contourite drift sector contains the Faro-Cadiz sheeted drift that evolves towards the west into huge mounded drifts (e.g., Faro Drift) separated from the upper slope by the Alvares Cabral contouritic moat (Fig. 1a).

After the Miocene-Pliocene boundary, the Strait of Gibraltar became the gateway for the MOW into the Atlantic and the CDS recorded a series of tectonic pulses of different cyclicity that defined three evolutionary stages (Hernández-Molina et al., 2016): (1) Initial-drift stage (Pliocene, 5.33-3.2 Ma). Sedimentation was dominated by downslope processes, mostly turbiditic and debris flows while the progressive strengthening of a relatively weak MOW deposited large muddy sheeted drifts; (2)

Transitional drift stage (late Pliocene-early Quaternary, 3.2-2 Ma). This stage was characterized by interbedded contourites and turbidites, and occasional debrites, indicating a progressive intensification of the MOW strength; and (3) Growth-drift stage (after 2 Ma). Bottom-current activity prevailed over downslope-trending processes and shaped the present-day Gulf of Cadiz Contourite Depositional System (Hernández-Molina et al., 2016). This last Quaternary stage includes three main phases (Llave et al., 2001, 2006, 2007a,b, 2011). From the Early Pleistocene to the Mid-Pleistocene the MU core flowed along the base of the upper slope and mounded and sheeted drifts were deposited on the upper-middle slope boundary. Between the Mid Pleistocene and the Late Pleistocene, the MU core migrated northward due to changes in the tectonic activity of the Guadalquivir Bank and the diapiric ridges. During this stage, the main MOW flow that was previously conducted through five channels at the exit of the Strait of Gibraltar migrated to its present-day location along the Southern channel (Llave et al., 2019). These oceanographic changes resulted in the formation of mixed drifts, involving interaction between bottom current activity and gravitational processes that buried part of the sheeted and mounded drifts. During the Late Pleistocene to Holocene, a further northward migration of the MU core, that flowed with a more tabular character connecting with the Northern channel, resulted from tectonic movements in the Strait of Gibraltar and the reactivation of diapiric bodies, while the Southern Channel maintained its present-day position (Llave et al., 2019). During this stage the Gusano and Huelva channels were excavated on the proximal middle slope, and the mixed drifts were fossilized by a more aggrading plastered drift at the transition between the upper and middle slope. In this scenario, the MU core flow along the upper slope and upper terrace was favoured during warm highstand intervals, whereas the Lower core flow predominated along the middle slope, or even in deeper depths, during cold lowstand intervals (Llave et al., 2007a,b; Hernández-Molina et al., 2014; Lofi et al., 2016).

2.4. The Gulf of Cadiz upper slope

The upper slope along the Gulf of Cadiz has only been partially studied so far. The SE part of the northern Gulf of Cadiz upper slope is dominated by plastered contourite drifts incised by erosive scarps (Nelson et al., 1993, 1999; Llave et al., 2007b; Hernández-Molina et al., 2014; Brackenridge et al., 2018). The plastered drift along the Cadiz upper slope is composed of highly bioturbated silts to sandy silts and displays characteristic bi-gradational sequences (Brackenridge et al., 2018), and results from the interplay of bottom currents and turbidity currents/spillover processes as the main sediment supply (Nelson et al., 1993, 1999; Hernández-Molina et al., 2014; Alonso et al., 2016). The upper slope in this area is incised by numerous gullies that have been studied from a geostatistical point of view and related to gravitational flows since the Last Glacial Maximum, fed from the Guadalquivir and Guadalete rivers and mass wasting sediment supply (Fernández-Salas et al., 2015; Sánchez-Rubio et al.,

206 2015). Deposits belonging to regressive and lowstand systems tracts and accumulated during the Late
207 Quaternary compose the middle to lower slope sequences (Rodero et al., 1999; Mestdagh et al., 2019).
208 Towards the NW, the upper slope becomes the erosional northern wall of the Alvares Cabral
209 contourite moat (Faugères et al., 1984; Llave et al., 2001; García et al., 2009; Roque et al., 2012; Fig.
210 1a). The westernmost upper slope, in the Portuguese margin, is dominated by the interplay between
211 contouritic and turbiditic processes, with the incision of the Portimão, Lagos and Sagres submarine
212 canyons in the contourite-dominated middle slope and down to the deeper basin (Mulder et al., 2006;
213 Marchès et al., 2007, 2010; Fig. 1a).

214 **3. Datasets, methodology and nomenclature**

215 *3.1. Datasets and methodology*

216 This work analyses geophysical and geological datasets with different degrees of resolution (Fig.
217 1b). The regional bathymetry has a resolution of 500 m and has been obtained from the GMRT Map
218 Tool (Ryan et al., 2009). The study area is covered with a high-resolution swath bathymetry data
219 compiled along a series of cruises (SWIM compilation, Diez et al., 2005; CONTOURIBER, MOWER,
220 INDEMARES) and gridded at a resolution of 50 m. Visualization and interpretation of bathymetric data
221 were achieved using Fledermaus, Global Mapper and Mirone softwares. Airgun profiles were acquired
222 during the CONTOURIBER and MOWER cruises. They are oriented NNW-SSE and WNW-ESE. Airgun 2-D
223 seismic reflection profiles were acquired using different arrangements of 610-910 cu.in GI-airguns
224 adapted to the water depth and quality of the signal. Shot frequency was 6 seconds and sampling rate
225 of 0.5 ms. During the cruises navigation was controlled by the EIVA NaviPac and the vessel was
226 positioned with a GPS dynamic system. The data were acquired with a three-channel (40
227 receivers/channel), 250 m long SIG streamer and recorded with a DELPH system. The vertical
228 resolution of the seismic profiles is less than 10 m. Processing was performed with the Hotshots
229 software and followed standard procedure, including equalization, low frequency filtering, band-pass
230 filtering, stacking, and resampling to 1 ms. A grid of NE-SW and NW-SE-oriented multichannel 2-D
231 seismic reflection profiles were provided by Repsol-YPF (S81). The entire seismic data set has been
232 visualized and interpreted using the Kingdom Suite software.

233 High-resolution data (bathymetry and seismic profiles) have been analyzed in order to characterize
234 the morphological features. To study the late Quaternary evolution of the upper slope, airgun seismic
235 profiles have been correlated with previous regional stratigraphic studies based on the analysis of
236 multichannel 2-D seismic reflection profiles (Hernández-Molina et al., 2016; Figs. 1b and 3). Two major
237 unconformities (Mid Pleistocene Discontinuity, MPD and Late Quaternary Discontinuity, LQD) were
238 identified after the Integrated Ocean Drilling Program (IODP) Expedition 339 and with the additional

information from well MPC-1 located in the upper slope of the studied area (Hernández-Molina et al., 2016). Despite the different resolution, these horizons can be translated to the dataset used in this study (Fig. 3). The seismic units correspond to the most recent Quaternary units (QIII) identified by Hernández-Molina et al. (2016) and QII (Llave et al., 2001, 2007, 2011; Brackenridge et al., 2013). The MPD has also been interpreted in previous studies (Fig. 3) as the Mid Pleistocene Revolution discontinuity (Llave et al., 2001, 2007, 2011; Hernández-Molina et al., 2003, 2006; Brackenridge et al., 2013), D2 (Marchès et al., 2010) or H4 (Roque et al., 2012). The discontinuity bounding units Q5 and Q6 correlates with discontinuities LQD (Hernández-Molina et al., 2016), D3 (Marchès et al., 2010) and H5 (Roque et al., 2012). The analysis of multichannel seismic profiles has allowed controlling the slope sedimentary evolution, and to analyze the structural features affecting the sediment record. The analysis of high-resolution seismic profiles (airgun) has allowed a more detailed characterization of the geometry, distribution and character of the seismic units in a temporal scale from the Middle Pleistocene to present. The penetration of these profiles and the presence of the bottom multiple reflection only allows a detailed description of the most recent unit, Q6. In addition, the multichannel seismic profiles have been used to obtain isochore maps of the seismic units identified in this work.

3.2. Nomenclature

Morphological features are identified based on their morphometric parameters, spatial distribution and seismic characteristics. Contouritic morphological features (contourite drifts, channels, furrows, terraces) follow the nomenclature established by Faugères et al. (1993a,b, 1999), García et al. (2009) and summarized by Rebesco et al. (2014). Sediment waves are identified based on the bathymetry and on their internal geometry observed in seismic profiles, with changes in the thickness of individual seismic layers (Berndt et al., 2006; Viana, 2009). Mass transport deposits (MTDs) are defined based on their seismic signature including a basal erosional surface, top hummocky relief at the top and internal chaotic to transparent seismic facies (Shanmugam, 2007; Posamentier and Martinsen, 2010; Shanmugam, 2012; Ruano et al., 2014). Mass movement erosional features include submarine valleys and escarpments. Upper slope valleys are classified as gullies, based on their downslope trend (Fedele and Garcia, 2009), and their dimensions -an order of magnitude smaller than submarine canyons (Field et al., 1999; Rinke-Hardekopft et al., 2018). Shelf-edge escarpments are interpreted as slide scars based on their arcuate-linear shape and their step-like profiles that truncate underlying seismic reflections (Mulder and Cochonat, 1996; McAdoo et al., 2000; Twichell et al., 2009; Piper et al., 2012; García et al., 2016). Fluid-escape features are defined by their circular- to elliptical plan-view shape in the seafloor (Hovland and Judd, 1988; Schattner et al., 2018), their characteristic seismic signature (Cartwright and Santamarina, 2015) and based on previous descriptions (Baraza and Ercilla, 1996; Baraza et al., 1999).

4. Results

4.1. Physiography and morphology

4.1.1. Physiography

The continental margin close to the Strait of Gibraltar extends for about 100 km with a SSE-NNW-orientation, turning to a ESE-WNW orientation off the Guadalquivir river mouth (Figs. 1a and 4a). The continental shelf-edge in this proximal part of the margin is relatively smooth along the study area and occurs at water depths of 110-130 m. The upper slope reaches depths of 390-480 m, extending deeper in the area off Cadiz, to the east of the Cadiz diapiric ridge (green profiles in Fig. 4b). The upper slope profile is flat to convex-upward in the south and central part of the study area and flat to concave-upwards in the north (Fig. 4b). A marked change in the slope gradient marks the transition between upper and middle slope except for the central part of the study area, where the transition is smooth and bulge-shaped (Fig. 4b).

In the studied sector (Figs. 4 and 5) the physiography of the upper and middle slope allows the establishment of three areas with distinct bathymetric profiles: Southern, Central and Northern (Fig. 4a). The Southern area displays a featureless upper slope with a convex-upwards profile and widths of about 16 km (Fig. 4b). Its lower limit, at about 500 mwd, connects with a narrow and steep ramp (2 km wide and 3º slope gradient) that connects with the Northern contourite channel in the middle slope. The channel is incised at the western part of a 35 km wide terraced platform at 670-770 mwd that limits towards the NW with the Cadiz and Huelva contourite channels (Fig. 4a). The Central area shows a relatively flat upper slope profile, with width increasing towards the north from about 5 km to a maximum of 22 km, whereas the steepness decreases from about 3° to 1.2° (Fig. 4b). The connection with the Northern channel in the middle slope occurs at water depths of about 500 m through a steep ramp (< 1 km wide and up to 7°) (Fig. 4b). The Northern area has a convex-upward upper slope with a width that decreases towards the north to about 12 km, and the steepness ranges between 1 and 2.2° (Fig. 4b). It connects smoothly with the middle slope at water depths of 400-450 m. The middle slope has a lower gradient (less than 0.7º) and connects with the Faro-Cadiz sheeted drift at the eastern side of the Cadiz diapiric ridge. The sheeted drift is bounded towards the west by the Tofiño contourite channel and the Cadiz diapiric ridge and to the south by the Huelva contourite channel (Fig. 4b).

4.1.2. Morphological features

A range of morphological features have been identified in the study area, and are classified according to their origin as (i) structural, including the diapiric highs and ridges, (ii) contouritic,

represented by a large plastered drift, sediment waves and contourite channels, (iii) gravitational, including escarpments and gullies , and (iv) fluid-escape related features.

(i) Structural features. The Cadiz diapiric ridge (CDR; Figs. 4a and 5b) is the main outcropping diapiric feature in the study area. The ridge has an N-S to NNE-SSW orientation. Its northern part outcrops in the middle slope close to the limit with the upper slope in the Northern area and is dissected by the Gusano and Tofiño contourite channels. The southern part lies between the Huelva and Cadiz contourite channels. The ridge has isolated peaks up to about 200 m in height, with a minimum water depth of 320 m.

(ii) Morphological features of contouritic origin. The *plastered drift* that makes up the upper slope (Hernández-Molina et al., 2014; Brakenridge et al., 2018) has a typical convex-upwards morphology, and the rest of morphological features are overprinted on its relatively flat surface (Fig. 4). *Sediment waves* are superimposed on the plastered drift in the Northern area. They are oriented SE-NW to S-N (parallel to slightly oblique to the isobaths; Fig. 5c). Individual crests are around 0.5-1 km long, and the wavelength averages 0.5 km. Sediment waves are asymmetric, with steeper downslope-facing flanks (up to 2.4º) and almost flat upslope-facing flanks. C*ontourite channels* (Northern, Southern, Cadiz, Huelva, Gusano and Tofiño) are major erosional features composing the Gulf of Cadiz Contourite depositional system (Hernández-Molina et al., 2003; García et al., 2009; Lozano et al., 2020). The upper slope connects with the Northern channel defined by Hernández-Molina et al. (2014) at 530-580 mwd in the Southern and Central areas (Fig. 5b). The Northern channel joins the Huelva and Cadiz contourite channels along the distal limit of the upper slope and is absent in the Northern area of this study (Fig. 4a).

(iii) Gravitational features. *Shelf-edge escarpments* occur in the Central and Northern areas (Figs. 5b and 5d). A prominent arcuate escarpment at the shelf-edge of the Central area is 20 m high and about 4 km long. Basinwards of the escarpment the bathymetric profile is concave-upwards (Fig. 5d). Linear, up to 8 m high N-S to NW-SE-oriented escarpments occur along the shelf-edge of the Northern area. A 12 km long linear escarpment 30 m deep and 5º steep occurs in the Southern area at the limit with the Northern channel, where the channel trend changes from SSE-NNW to SE-NW (Fig. 5b). G*ullies* occur on the Central and Northern areas (Fig. 5b). Gullies in the Central area extend from 205-250 mwd, below the continental shelf-edge, to the rim of the Northern channel. Gullies are generally asymmetric, with steeper and higher NW walls and present V-shaped profiles (Fig. 5e), 12-20 km long, 2-25 m deep and 0.2-1 km wide. Their orientations range ENE-WSW to NE-SW, they are spaced 0.4-2 km and display a dendritic convergent pattern (Fig. 5b). Gullies are less common in the Northern area. Their heads are located at 205-240 m, and they terminate at water depths of 405-415 m, in the

relatively flat Faro-Cadiz sheeted drift on the middle slope (Fig. 5b). They are smaller (5.5-9.5 km long; 0.2-0.4 km wide and 1-3 m deep) than in the Central area and have asymmetric U- or V-shaped profiles (Fig. 5e). They are E-W to ENE-WSW-oriented, with linear trends and they occur as individual features, spaced 0.3-1 km.

(iv) Fluid-escape features are circular- to elliptical-shaped depressions identified in the deeper part of the upper slope in the Central area close to the rim of the Northern channel (Fig. 5b). They are up to 1.5 km wide and 70 m deep. Most of them are aligned along the axes of gullies and their long axis have similar orientations (roughly NNE-SSW) whereas others occur in inter-gullies areas and are oriented parallel to the bathymetric contours.

4.2. Seismic analysis

4.2.1. Acoustic basement and structural features

The topography of the acoustic basement in the study area is highly irregular, with depths ranging between 0.5 and 3.7 s two-way travel time (TWTT; Fig. 6a). A prominent acoustic basement high in the SE part of the study area delimits a NE-SW-trending depression extending from the present-day continental shelf to the middle slope. Basement highs coincident with the Cadiz and Guadalquivir diapiric ridges delimit a second NE-SW oriented basement depression that opens towards the SW. Other minor basement highs roughly coincide with the present-day shelf-edge, whereas most of the upper slope is characterized by basement highs delimiting irregular depressions.

Diapir tops are spatially associated to the basement topography (Fig. 6a). Apart from the outcropping diapiric ridges, most diapirs are buried and their tops are aligned with two predominant orientations: NE-SW and NW-SE. The top ofmost of the upper slope buried diapirs as well as the two outcropping diapiric ridges are oriented NE-SW to ENE-WSW. Below the distal limit of the Central area a NE-SW diapir and its associated faults reach the seafloor. Columnar zones of acoustic amplitude anomalies and truncated seismic reflections connect vertically withthe circular- to elliptical-shaped fluid-escape depressions on the present-day sea-floor and in the seismic record (Figs. 5b, 7b and 8b). Some other diapirs are aligned in a perpendicular NW-SE to WNW-ESE direction (Fig. 6a). They occur in the present-day Cadiz contourite channel, in the upper slope of the Central area (where the heads of many gullies occur), on the upper slope at the limit between the Northern and Central areas (coinciding with the distal end of many gullies), and at the NW side of the outcropping Cadiz diapiric ridge, where the Gusano channel is excavated. Faults are widespread features in the sedimentary record of the Cadiz upper slope (Figs. 6b to 10). They are mostly normal faults that are rooted in the diapirs, both at their tops and flanks and can be defined as extensional crestal faults (Jackson and

Hudec, 2017). Faults rarely reach the seafloor, and are often associated to the gullies and to the fluid-escape features (Figs. 6b to 10).

4.2.2. Seismic stratigraphy

The two major seismic discontinuities (MPD- Mid Pleistocene Discontinuity and LQD- Late Quaternary Discontinuity) define two major late Quaternary units , following the most recent regional nomenclature proposed by Hernández-Molina et al. (2016) (Figs. 3c and 3d): a) Seismic Unit Q5 (MPD-LQD, subdivided into three sub-units, Q5-a to Q5-c) and b) Unit Q6 (LQD-Present, composed of four sub-units, Q6-a to Q6-d). All discontinuities are better defined in the proximal upper slope by pronounced changes in the frequency and acoustic amplitude of reflections. The character of units and sub-units and the main seismic features are shown in Figures 7 to 11. The topography of the basal discontinuities bounding each unit and their thickness distribution are shown in Figure 12.

a) Seismic Unit Q5: MPD-LQD

The seismic configuration of Q5 unit shows a mostly aggrading stacking pattern with parallel stratified reflections of medium to high amplitude and interlayered wavy-chaotic packages with disrupted reflections, in the Southern area (Figs. 7 to 9). The Central area shows layered and wavy-chaotic disrupted reflections that display a progradational configuration towards a paleo-channel about 6 km to the east of the present-day Northern channel (Fig. 10). In the Northern area, Q5 mostly presents parallel stratified reflections. V- or U-shaped erosional depressions are mostly identified in the seismic lines parallel to the bathymetric contours and occur mostly associated to diapir-related faults. They are more common in the top of the unit where they occur around diapiric highs in the Southern area and show vertical migration towards the NW (Fig. 8a). Q5 is deformed by the NE-SW and the NW-SE trending diapiric alignments and related faults, with upward tilting and thinning towards the diapiric highs (Figs. 7 to 11).

The overall distribution of Q5 is patchy, with depocenters up to 360 ms TWTT thick located between diapir highs and pronounced decreases in thickness towards the top of isolated diapiris and diapiric ridges (Fig. 12a). Depocenters are smaller in the Northern area, whereas the Central and Southern areas contain wider and thicker depocenters (230-360 ms TWTT) on the present-day shelf-edge and upper slope. The geometry of the seismic unit Q5 is tabular in the Southern and Central areas (Figs. 9 and 10). In the Central area, thickness decreases in a paleo-channel displaced about 6 km to the east of the present-day Northern channel. In the Northern area (Fig. 11), the geometry ranges from wedge-shaped, with higher thickness towards the proximal areas of the slope to lens-shaped, with minimum thickness towards the flanks of diapiric bodies. During deposition of Q5 the topography

of the upper slope changed significantly (MPD base surface to LQD base surface; Fig. 12b to 12d) producing: a) the infilling of the NE-SW-trending depressions at the SE of the study area and between CDR and GDR; b) the infilling of small depressions at the present-day base of the upper slope; c) the advance of the continental shelf-edge to positions similar to the present-day.

Three sub-units compose the seismic unit Q5 (Q5-a, Q5-b and Q5-c, from older to younger). The three sub-units have similar distribution patterns, with a progressive displacement of depocenters towards the present-day shelf-edge (Figs. 7 to 11). Q5-a (MPD-5b discontinuities) has mid to high acoustic amplitude in generally parallel layered reflections. It displays maximum thickness in the present-day shallower upper slope of the Central and Northern areas, and in the middle upper slope of the Northern area. Q5-b (5b-5c discontinuities) has lower acoustic amplitude than Q5-a and its depocenters are aligned along the present-day shallower upper slope of the Southern and Central areas. Q5-c (5c-LQD discontinuities) is characterized by low-acoustic ampitude at the base that become higher towards the top. Its thickness is higher along the shallower upper slope of the Central area, and on the midddle upper slope of the Southern area.

b) Seismic Unit Q6: LQD-seafloor

The seismic configuration of Q6 shows layered reflectors locally interbedded with packages of disruptedreflectionss in the Central and Northern areas, and lower acoustic amplitude than Q6 (Figs. 7 to 11). Q6 is widely deformed by NW-SE buried diapir alignments and the outcropping diapiric ridges, but deformation by NE-SW-oriented ones is drastically diminished. The NW-SE-oriented diapir alignment located in the limit between the Central and Northern areas only deforms Q6, whereas the underlying unit Q5 is not affected. Seismic unit Q6 is much less deformed by diapir-related faults than Q5, in particular towards the top (Figs. 7 to 11).

The overall distribution of Q6 is different from the underlying Q5, showing greater thickness (up to 660 ms TWTT) and a more homogeneous distribution (Fig. 12c). The main depocenter locates below the present-day shelf edge, at the limit between the Northern and Central areas. Thickness decreases towards the CDR and GDR and the buried NW-SE-oriented diapiric alignments at the eastern side of the CDR. The deposition of Q6 resulted in the growth of the present-day upper slope to the NE rim of the Northern contourite channel, that presents minimum thicknesses (<200 ms TWTT). Since the LQD, the main changes in the topography include the infilling of previous depressions, the excavation of the Gusano contourite channel to the north of the CDR and the incision of gullies (Fig. 12d).

Q6 is composed of four sub-units (Q6-a to Q6-d, from older to younger). Whereas the four sub-units show a similar pattern of deformation, their distribution, geometry and internal configuration have important differences and will be described individually.

Q6-a sub-unit (LQD – 6b discontinuity) has a tabular geometry with layered reflections in the Southern area. The unit displays increased thickness and disrupted reflections in the footwall side (basinward) of a set of diapir-related faults (Fig9 8). It displays maximum thickness of about 0.12 s TWTT in the Central area upper slope at the footwall side of a set of diapir-related faults. Thickness is significantly low in the shallower upper slope and particularly at the proximal middle slope, at the eastern side of a paleo-channel, slightly displaced to the west of the present-day Northern channel (Fig. 10). V- and U-shaped depressions occur both within the sub-unit and incised in the top discontinuity, generally associated to faults (Figs. 7b and 8a). Towards the Northern area, Q6-a shows layered reflections with V-and U-shaped depressions in the deeper areas between diapirs, and the thickness is generally low (Figs. 7 and 8). This sub-unit is generally thin with maximum thickness of about 180 ms TWTT in a wide depocenter on the deeper part of the present-day upper slope.

Q6-b (6b-6c discontinuities). This sub-unit displays similar seismic characteristics as Q6-a in the Southern area, but the depocenter is slightly displaced upslope (Fig. 9). In the Central area the upslope displacement of the deposition is more evident as well as a thickness decrease below the present-day Northern channel (Fig. 10). In the Northern area the base of the sub-unit has a transparent to chaotic character with disrupted reflections (Figs. 7 and 11). The sub-unit presents numerous small V-shaped depressions in the deepest part of the upper slope and thickness increases significantly between diapiric highs.

Q6-c (6c-6d discontinuities). This sub-unit is mostly layered in the entire study area. The top boundary shows erosional truncations in the Southern area. It presents few V- or U-shaped depressions in the Central area, in most cases associated with faults (Figs. 7 and 10). In this area, Q6-c displays mounded configurations with upslope progradation on the deeper part of the upper slope, at the foot wall of a set of diapir-related faults (detail in Fig. 10). In the Northern area V- and U-shaped depressions only occur at the top boundary (Fig. 11). Q6-c is relatively thin, particularly in the Southern area. Maximum thickness (around 0.2 s TWTT) occur in the Central area where the distribution is affected by the diapiric highs. The Northern area shows depocenters in the depressions between diapiric highs.

Q6-d (6d discontinuity- seafloor) displays a stratified character with very low acoustic amplitudes in in the Southern and Central areas (Figs. 9 and 10). In the Central area layered reflections are cut by V-shaped depressions along the entire sub-unit that show a NW upward migration (Fig. 8). Q6-d displays

a distinctive wavy-chaotic seismic character with disrupted reflections at the shallower upper slope in the Northern area and chaotic-transparent in the deeper parts where it connects with the middle slope (Fig. 11). The main depocenters occur at shallower depths than the previous sub-units, along the present-day shelf-edge in the Central area.

5. Discussion

The physiographic, morphologic and seismic stratigraphic analysis presented in the previous sections allow inferring the sedimentary processes that have shaped the upper slope and proximal middle slope of the Gulf of Cadiz in the study area and to analyze their evolution since the MPD based in chronostratigraphic correlations. Two major factors (sea-level changes and episodic tectonic activity) are proposed to have controlled the sedimentary evolution of this part of the margin.

5.1. Sedimentary interpretation and chronostratigraphic correlations

Based on the results of this work and on previous published literature (Nelson et al., 1993, 1999; Llave et al., 2007b; Hernández-Molina et al., 2014; Brackenridge et al., 2018), the upper slope is characterized by plastered drift deposition since the MPD, as suggested by the parallel-stratified seismic character of high lateral continuity, aggrading pattern and tabular to slightly mounded geometry (Faugères et al., 1999; Hernández-Molina et al., 2006; Van Rooij et al., 2010). At the connection with the middle slope, the plastered drift limits with the Northern channel (Hernández-Molina et al., 2014) that can be defined as a contourite channel based on the along-slope trend and the presence of truncated reflections (Figs. 4, 5 and 9 to 11; Faugères et al., 1999).

The LQD marks a change in the stacking pattern as the plastered drift-contourite channel system migrated towards the SW, the plastered drift increased in thickness and the contourite paleo-channel increased its incision in the proximal middle slope (Fig. 12). The chronostratigraphic correlation allows interpreting the sedimentary evolution in relation with the two main discontinuities, the MPD and the LQD. The MPD (base of seismic unit Q5) is a discontinuity that exhibits different stratigraphic character in the Gulf of Cadiz continental slope, such as an erosive hiatus, a condensed section or a section with reduced sedimentation rate in different locations, related to a tectonic event related with tectonic shortening and gravitational spreading, with an age around 0.7–0.9 Ma (Hernández-Molina et al., 2016; Lofi et al., 2016). It also corresponds to the Mid Pleistocene Revolution (MPR) in the quaternary climatic discontinuity, related to the first important cold event and associated sea-level fall in the Pleistocene (Llave et al., 2001, 2004; Hayward et al., 2005; Head and Gibbard, 2005; Ehlers and Gibbard, 2007) and the MOW enhacement coeval with an increase in the sedimentation rates in the Gulf of Cadiz (Llave et al., 2011; Roque et al., 2012; Hernández-Molina et al., 2016). LQD corresponds to a hiatus in the time window of 0.3–0.6 Ma (Hernández-Molina et al., 2016; Lofi et al., 2016)

497 characterized in seismic profiles of the middle slope contourite drifts by an angular unconformity on
498 the basin margins and the flanks of the topographic highs that changes laterally to concordant
499 relationships in the middle of the basins (Hernández-Molina et al., 2016). This discontinuity has been
500 associated with a lowering of the sea level (Marchés et al., 2010) and an strenghtening of the MOW
501 circulation in the middle continental slope (Roque et al., 2012).

502 *5.2. Influence of sea-level on sedimentation: paleoclimatic and paleoceanographic implications*

503 Sea-level change is a crucial factor controlling bottom current sedimentary processes (Rebesco et al.,
504 2014). The stacking pattern of the plastered drift and the adjacent Northern contourite channel allows
505 inferring the paleoclimatic and paleoceanographic conditions that influenced their evolution. The
506 results of this study suggest that the plastered drift grew under the activity of a weak ENACW flow,
507 whereas the contourite paleo-channel evolved by the erosive effect of the MOW, during regressive
508 and lowstand sea-level stages. Lowered sea-levels during glacial stages are characterized by enhanced
509 deep circulation that produces a more intense and deeper ML in the Gulf of Cadiz (e.g. Llave et al.,
510 2006, 2007, Toucanne et al., 2007; Marchès et al., 2010; Lofi et al., 2016) and even the probable
511 dissappearance of the MU (Roque et al., 2012). Since the study area is located at the present-day
512 interface between the MOW and the ENACW (Fig. 2), the deepening of the MOW would have left the
513 entire upper slope under the effect of the ENACW during the lowstands of the asymmetric glacial
514 cycles. This scenario would last a longer period of time compared with the highstand situation in which
515 the MOW covers the upper slope, as at present. Furthermore, it is during sea-level lowstands that the
516 sediment supply from fluvial discharge and continental shelf, required to produce significant plastered
517 drift growth in this area is enhanced (Rodero et al., 1999; Mestdagh et al., 2019). Under this
518 assumption, sub-unit boundaries within Q5 and Q6 units can be tentatively linked to the 100 ky
519 Quaternary climatic oscillations as defined by the benthic $d^{18}O$ isotopic curve of Lisiecki and Raymo
520 (2005) (Fig. 3d).

521 V- and U-shaped depressions not related to diapir-associated faults are widespread along the seismic
522 sub-units (Fig. 3d) and we interpret them as paleo-gullies, based on the truncated reflections in their
523 flanks, the local presence of lateral deposits (levees) and their morphological resemblance with the
524 present-day gullies. Their occurrence supports that the bulk of the plastered drift growth affected by
525 gullies incision occurred during glacial climatic stages, assuming a genetic link between gully formation
526 and sea-level lowstands, as documented in other continental margins (Field et al., 1999; Spinelli and
527 Field, 2001). Gullies migration suggests southeastward bottom current activity, coincident with the
528 circulation pattern of the ENACW, based on the results of recent three-dimensional flume-tank
529 experiments (Miramontes et al., 2020). These experiments demonstrate that the direction of

migration of turbidite channels is opposite to the direction of the bottom current interacting with them. During transgressive and highstand stages the study area is, in contrast, under the influence of the MOW (Sánchez-Leal et al., 2017). In these conditions, such as present-day, the plastered drift is reworked by the northeast-trending flow, most gullies become inactive and the contourite channel is strongly affected by the MU flow. The vertical shifts along the glacial/interglacial cycle of the interface between the Mediterranean Water and the overlying ENACW (Fig. 2; Hernández-Molina et al., 2014, 2016; Sánchez Leal et al., 2017) and the high variability of the water masses dynamics (Bellanco and Sánchez-Leal, 2016; Roque et al., 2019) may also have favoured the incision of gullies.

LQD marks a change in the paleoclimatic and paleoceanographic conditions that influenced the evolution of the plastered drift. After the initial stage of plastered drift growth and upslope migration (Q6-a and Q6-b), a stage of aggradation occurred with deposition of the two more recent sub-units Q6-c and Q6-d (Fig. 10). The most recent sub-unit Q6-d is incised by markedly asymmetric gullies displaying northwestward migration in the Central area, which denotes increased bottom current influence on the gravitational sediment transport. The predominance of contouritic processes versus gravitational processes during deposition of this last sub-unit is also responsible for the inactivation and infilling of many buried upper slope gullies. The mounded body infilling the erosional scour at the shelf edge (Fig. 9b) suggests bottom current acceleration by the interaction with the escarpment associated to the escarpment (e.g., Rebesco et al., 2014; Juan et al., 2020). The deposition of a sediment wave field in the Northern area, which constitutes the main morphological difference with the Central area (smooth inter-gullies areas; Fig. 5), is interpreted as a combination of sediment deformation related to unconfined turbidite flows (Ercilla et al., 2002; García et al., 2012) and the intensified effect of bottom currents (Faugères et al., 2000a,b; Gonthier et al., 2002), as indicated by the orientation (parallel to oblique to bathymetric contours and to the bottom current direction) and the upslope migration of sediment waves (Masson et al., 2002; Wynn and Stow, 2002). Bottom currents intensification after the LQD may have been favored by the prevalence of glacial cycles with longer and warmer interglacials (Roque et al., 2012), and is consistent with the transition from sandy sheeted drifts to muddy sheeted and mounded drifts observed in the middle slope (Hernández-Molina et al., 2016). Sediment waves development may also have been favored by high-energy processes (eddies, internal tides or internal waves) associated to water masses interfaces (Cacchione et al., 2002; Youbin et al., 2008; Lamb, 2014) as their location also coincides with the interface between the ENACW and the MU (Fig. 3; Hernández-Molina et al., 2014, 2016; Sánchez-Leal et al., 2017: Roque et al., 2019).

562 *5.3. Episodic pattern of tectonic deformation: Influence of tectonic deformation on sedimentary*
563 *processes*

564 The MPD marked a phase of tectonic activity in the region that resulted in the formation of
565 erosional surfaces close to diapirs and basement highs (Lofi et al., 2016; Hernández-Molina et al.,
566 2016). Tectonic activity evolved episodically since the MPD as shown by changes in the deformation of
567 seismic units and sub-units and the different development of morphological features in the seismic
568 record. During deposition of Q5 (MPD-LQD) sedimentation was controlled by the activity of marly and
569 salt diapirs rooted in the AUGC, under a compressive regime between Iberia and Africa (Maestro et al.,
570 2003; Medialdea et al., 2004), as indicated by the correlation between diapir distribution (Fig. 6) and
571 the thickness of seismic unit Q5 which infills depressed areas delimited by diapiric highs (Fig. 12a). The
572 upward deformation and thinning of sub-units indicate that diapir activity was coeval to Q5 deposition.

573 A prominent change of depositional conditions during deposition of sub-units Q6-a and Q6-b (LQD-
574 discontinuity 6c) is inferred by the absence of significant thickness variations in relation to NE-SW-
575 aligned buried diapirs in the upper slope, that would have become inactive (Figs. 7 to 11). The
576 decrease in diapiric activity in the upper slope may be coeval with the inactivation of some diapiric
577 ridges in the middle slope (Hernández-Molina et al., 2016). In contrast, the outcropping Cadiz diapiric
578 ridge (CDR) and the buried NW-SE-aligned diapirs continued or started to deform the sedimentary
579 units. In this scenario, mass flow deposits were formed at the foot of diapir-related faults (Figs. 9and
580 10).

581 Tectonic activity can be related to the WNW-ESE strike-slip faults recognized in the Gulf of Cadiz,
582 with a dextral movement (Terrinha et al., 2009; García et al., 2009; Bartolomé et al., 2012; Martínez-
583 Loriente et al., 2014). During this stage (Q6-c) sedimentation changed drastically as it lacks most of the
584 structural imprint in the form of faults related to diapirs, except for the southernmost part of the study
585 area. In this scenario, mass flow deposits were formed at the foot of the faults. Although the
586 continuous uplift of NW-SE-oriented diapirs is suggested by the thinning of the sub-unit Q6-c on top of
587 the diapiric highs, it is less significant than in the other stages (Figs. 7 to 11). After the scarce diapiric
588 activity in the previous phase, deformation in sub-unit Q6-d is related to the activity of the
589 outcropping diapiric ridges and the buried NW-SE-oriented diapirs. This activity may explain the
590 instability event that created escarpments and the erosion of the previous sub-unit in the Southern
591 area (Fig. 10). The last sub-unit of Q6 (Q6-d; discontinuity 6d-surface) is only deformed by the CDR and
592 one of the NW-SE-oriented diapir alignments located in the area that limits the Central and Northern
593 areas. The outcropping Cadiz and Guadalquivir diapiric ridges are the only NE-SW structures that show
594 significant activity after the MPD. This can be explained by changes in the activity of faults, leading to a

595 northwestward displacement of tectonic activity after the MPD, but can be also favoured by
596 downbuilding (passive diapirism), that allows the continued growth of a diapir after it pierces the
597 surface, while sedimentat accumulates at its flanks (Barton, 1933; Jackson and Hudec, 2017). The
598 relative high/low sedimentation rate around/on the diapiric ridges, caused by the activity of bottom
599 currents, would originate the differential sedimentary burden, contributing to diapir growth.

600 Episodic tectonic deformation has influenced the sedimentary processes since the MPD, including: 1)
601 bottom current deposition/erosion; 2) gravitational processes; and 3) fluid escape processes.

602 5.3.1. Tectonic influence on bottom current processes

603 Between the MPD and the LQD (seismic unit Q5) the plastered drift was deposited on the upper
604 slope, consisting of quite tabular and aggrading sub-units. Tectonic activity controlled the
605 accommodation space, as indicated by the distribution of depocenters in the depressions between
606 diapiric bodies (Fig. 12a). The paleo-channel was located about 6 km to the east from the present-day
607 Northern channel, whereas a wide terrace formed by gently upslope-prograding reflections was
608 deposited on the middle slope (Fig. 10a).

609 After the LQD, a number of processes including paleo-channel migration towards its present-day
610 position, the narrowing and/or westward displacement of the middle slope terrace and the basinward
611 migration of the plastered drift (Figs 7 to 12) could be related to tectonic activity of diapir-related
612 faults coeval with LQD. Diapiric activity uplifted the area bounding the Central and Northern areas. The
613 terrace-paleo-channel system migrated to a more distal position as it adjusted to the new margin
614 morphology, in a cooler climatic regime with probably deeper MOW/ENACW circulation. After the LQD
615 the plastered drift growth increased and depocenters migrated downslope, initially in the Central area
616 (sub-unit Q6-a; Fig. 10) and later in the Northern area (sub-unit Q6-b; Fig. 11). The plastered drift
617 growth is responsible for the unusual convex-upwards profile of the upper slope in the Central area
618 (Fig. 4b), that differs from the concave-upwards profile with marked gradient change between the
619 upper and middle slope in the rest of the margin. These lateral differences on the overall plastered
620 drift morphology could be explained by the relative higher dominance of gravitational processes over
621 bottom current processes along the upper slope. After the main pulse of basinward migration,
622 depocenters show a progressive displacement towards shallower positions (Figs. 10 and 11), in
623 agreement with the typical evolution of plastered drifts (Rebesco et al., 2014).

624 5.3.2. Tectonic influence on gravitational processes

Diapiric activity may be invoked as a trigger for mass-wasting processes, as uplift and faulting associated with diapir intrusion may produce fracture and oversteepening of the slope that leads to instability and failure (Cashman and Popenoe, 1985; Hampton et al., 1996). In the Cadiz upper slope, arcuate- and linear-shaped escarpments along the shelf-edge can be related to the activity of a buried diapir high and associated normal faults identified below in the sub-surface (Fig. 6). Moreover, the increase in upper slope gradient induced by diapirs uplift can further favor gully incision (Mountjoy et al., 2009; Argnani et al., 2011; Alves et al., 2014) as it is observed in the Central area. Furthermore, diapir-rooted faults may produce topographic steps or lips along which gravitational flows are channelized (Vargas et al., 2012; Micallef et al., 2014; Pellegrini et al., 2016; Tsai et al., 2018). This is proposed to be the case of the gullies in the older seismic unit Q5, particularly in the Central area, based on their spatial correlation with faults (Figs. 7 and 8). Subsequently, several Late Pleistocene and Holocene reactivations of upper slope diapirism (Vázquez et al., 2010; Fernández-Puga et al., 2014) could have favored continued gully development (Figs. 7 to 11), particularly in sub-unit Q6-c where gullies are less developed and only occur associated to diapiric highsic movements in the southern part of the study area (Fig. 8a). Uplift of the Cadiz diapiric ridge forced the confinement of mass transport deposits that occur as transparent to chaotic deposits in the most recent sub-unit Q6-d on the shallower upper slope and at the limit between upper and middle slope in the Northern area (Fig. 11), and may also have limited the gullies development in this area due to the decrease of the slope gradient.

5.3.3. Tectonic influence on fluid escape processes

Fluid-escape features include circular- to elliptical-shaped depressions on the seafloor and depressions in the seismic records (Figs. 7b and 8b). Depressions are distinguished from gullies based on the circular- to elliptical plan-view shape for the seafloor features (Hovland and Judd, 1988; Schattner et al., 2018), and the occurrence of acoustic amplitude anomalies in columnar shape and bright spots in the seismic record (Plaza-Faverola et al., 2011; Cartwright and Santamarina, 2015; Maestrelli et al., 2017). Indeed, evidences for fluid-escape related to active diapirism have been found in the Gulf of Cadiz, resulting in the formation of pockmarks and blind valleys (Medialdea et al., 2009; León et al., 2010). Fluid-escape may be controlled by diapiric faults, that form preferential conduits (Casas et al., 2003; Somoza et al., 2003; Medialdea et al., 2004; Fernández-Puga et al., 2007; Medialdea et al., 2009; Schattner et al., 2018). Fluid-escape features in the deeper upper slope of the Southern area (Figs. 5b, 7a and 8b) are located on top of buried diapir alignments that became inactive during the LQD, although recent fluid-escape activity has been demonstrated by the identification of seeping bubbles above some of the depressions (Baraza and Ercilla, 1996).

6. Summary and conclusions

The Cadiz upper and proximal middle slope have evolved since the Middle Pleistocene under the major control of the tectonic activity, responsible for diapiric movements and associated faults, and sea-level changes, that have determined the interplay between downslope (gravitational) and along-slope (bottom current related) sedimentary processes. Two evolutionary stages are proposed (Fig. 13):

a) Small, plastered drift deposition under the activity of NE-SW-oriented diapiric ridges (MPD-LQD; Fig. 13a). A plastered drift developed in the Central area during the regressive and low sea-level stages of glacial cycles, as the MU deepened and the upper slope was swept by the southeastward flow of the ENACW. In the northern area, small patchy plastered drifts were deposited. The activity of NE-SW-oriented diapiric bodies produced their deformation and the occurrence of mass flow processes such as slope instability and gullies incision. A contourite terrace associated to the main MOW flow was formed at the western side of the paleo-contourite channel.

b) Plastered drift growth and upslope migration of sedimentation under the activity of NW-SE-oriented buried diapirs (LQD-present; Fig. 13b). At the LQD, most of the NE-SW-aligned buried diapirs in the Central and Northern areas became inactive, but the activity of the outcropping diapiric ridges and the buried NW-SE-aligned diapirs resulted in deformation of the deposits by faults and the occurrence of mass-transport deposits related to slope instability. The results of this work suggest that adjustment to the tectonic uplift of the area bounding the Central and Northern areas produced the migration of the upper slope plastered drift and the terrace-channel system in the middle slope towards its present-day position. The plastered drift developed significantly during this stage, probably as result of deep currents enhancement and increased sediment supply during regressive and low sea-level stages. Seismic unit Q6 records the upslope migration of the plastered drift. Tectonic activity was not continuous, but a period of "quietness" led to low deformation and gully incision during deposition ofsub-unit Q6-c. This quiet period was followed by renewed tectonic activity of the outcropping diapiric ridges and the NW-SE-oriented buried diapiric bodies, which produced instability events.

This work reveals a progressive change in diapiric activity, both in the orientation of active diapir alignments along time and in the overall northwestward migration of deformation that is related with the dynamics of the Allocthonous Unit of the Gulf of Cadiz. Diapiric deformation produced changes in the accommodation space that was infilled by the predominant contouritic sedimentation, but also changes in the upper slope physiography, that led to the occurrence of a variety of downslope mass transport processes. The most important implications are: I) gullies incision favoured by the increase in the slope and controlled by diapir-related faults, affected along their development by the

691 southeastward bottom currents; II) mass transport processes related to the activity of diapir-related
692 faults and probably further facilitated by the erosive effect of the bottom current; III) fluid-escape
693 features associated to faults rooted in the diapirs; IV) changes in the bottom current distribution,
694 forced to adjust to tectonically-induced changes in the margin morphology.

695 The results of this work highlight the two-ways-interaction between diapiric activity and
696 erosive/depositional bottom current related processes. Sedimentation in the Cadiz upper slope since
697 the Middle Pleistocene is strongly controlled by the activity of buried diapirs that accommodate the
698 ongoing deformation of the Allochtonous Unit. The continuous deformation of the outcropping diapirs
699 after the LQD, when most of the buried NE-SW-oriented structures were inactivated, may result from
700 their passive behavior favored by the lack of sedimentary cover, that in turns is the result of bottom
701 currents activity sweeping the study area, producing the erosion/non deposition over diapiric ridges
702 and the development of thick contouritic drifts in the areas between diapirs. Together with sea-level
703 changes, recent tectonic deformation is demonstrated as a key control in the development of
704 contouritic-gravitational systems, and has to be incorporated in the investigation of their reservoir
705 potential.

706 **Acknowledgements**

707 This work has been possible thanks to funding provided by the following projects funded by the
708 Spanish Ministry of Economy and Competitivity: TALUS (CGL2015-74216-JIN), INPULSE (CTM2016-
709 75129-C3-1-R), CONTOURIBER (CTM2008-06399-04-04), MOWER (CTM-2012-395599-C03), SCORE
710 (CGL2016-80445-R; AEI/FEDER, UE), and FAUCES (CTM2015-65461-C2-1-R). We are very grateful to
711 REPSOL for allowing us to use an unpublished seismic line S81A-16 from the Gulf of Cadiz. The
712 investigation has been conducted within the framework of "The Drifters" Research Group (Royal
713 Holloway University of London). We are very grateful to Dr. Vittorio Maselli and Dr. Davide Gamboa for
714 their careful review of the manuscript and the helpful comments and suggestions. We also thank the
715 Associate Editor, Dr. Andrew Green, for his support in the publication process.

716 **Bibliography**

717 Akinci, L., Sawyer, D., 2016. Deriving the rate of salt rise at the Cape Fear slide using new seismic data.
718 In: Lamarche G. et al. (Eds.) Submarine Mass Movements and their Consequences. Advances in
719 Natural and Technological Hazards Research, Vol 41. Springer.
720 Alonso, B., Ercilla, G., Casas, D., Stow, D.A.V., Rodríguez-Tovar, F.J., Dorador, J., Hernández-Molina, F.J.,
721 2016. Contourite vs gravity-flow depostis of the Pleistocene Faro Drift (Gulf of Cadiz):
722 Sedimentological and mineralogical approaches. Marine Geology 377, 77–94.

723 Argnani, A., Tinti, S., Zaniboni, F., Pagnoni, G., Armigliato, A., Panetta, D., Tonini, R., 2011. The eastern
724 slope of the southern Adriatic basin: a case study of submarine landslide characterization and
725 tsunamigenic potential assessment. Marine Geophysical Research 32, 299–311.
726 Alves, T.M., Strasser, M., Moore, G.F., 2014. Erosional features as indicators of thrust fault activity
727 (Nankai Trough, Japan). Marine Geology 356, 5–18.
728 Baraza, J., Ercilla, G., Nelson, C.H., 1999. Potencial geological hazards on the Eastern Gulf of Cadiz slope
729 (SW Spain). Marine Geology 155, 191–215.
730 Baraza, J., Ercilla, G., 1996. Gas-charged sediments and large pockmark-like features on the Gulf of
731 Cadiz (SW Spain). Marine and Petroleum Geology 13, 253–261.
732 Baringer, M.O., Price, J.F., 1999. A review of the physical oceanography of the Mediterranean Outflow.
733 Marine Geology 155, 63–82.
734 Bartolome, R., Gràcia, E., Stich, D., Martínez-Loriente, S., Klaeschen, D., Mancilla, F., Lo Iacono, C.,
735 Dañobeitia, J.J., Zitellini, N., 2012. Evidence for active strike-slip faulting along the Eurasia-Africa
736 convergence zone: Implications for seismic hazard in the southwest Iberian margin. Geology 40,
737 495-498.
738 Barton, D.C., 1933. Mechanics of formation of salt domes with special reference to Gulf coast salt
739 domes of Texas and Louisiana American Association of Petroleum Geologist Bulletin 17, 1025–1083.
740 Bellanco, M.J., Sánchez-Leal., R.F., 2016. Spatial distribution and intra-anual variability of water masses
741 on the Eastern Gulf of Cadiz seabed. Continental Shelf Research 128, 26–35.
742 Berndt, C., Cattaneo, A., Szuman, M., Trincardi, F., Masson, D., 2006. Sedimentary structures offshore
743 Ortona, Adriatic Sea – Deformation or sediment waves? Marine Geology 234, 261–270.
744 Borenäs, K.M., Wåhlin, A.K., Ambar, I., Serra, N., 2002. The Mediterranean outflow splitting- a
745 comparison between theoretical models and CANIGO data. Deep-Sea Research II 49, 4195–4205.
746 Brackenridge, R.E., Hernández-Molina, F.J., Stow, D.A.V., Llave, E., 2013. A Pliocene mixed contourite–
747 turbidite system offshore the Algarve Margin, Gulf of Cadiz: Seismic response, margin evolution and
748 reservoir implications. Marine and Petroleum Geology 46, 36–50.
749 Brackenridge, R.E., Stow, D.A.V., Hernández-Molina, F.J., Jones, C., Mena, A., Alejo, I., Ducassou, E.,
750 Llave, E., Ercilla, G., Nombela, M.A., Pérez-Arlucea, M., Frances, G., 2018. Textural characteristics
751 and facies of sand-rich contourite depositional systems. Sedimentology 65, 2223–2252.
752 Cacchione, D.A., Pratson, L.F., Ogston, A.S., 2002. The shaping of continental slopes by internal tides.
753 Science 296(5568), 724–727.
754 Carter, L., Carter, R.M., 1988. Late Quaternary development of left-bank-dominant levees in the
755 Bounty Trough, New Zealand. Marine Geology 78, 185–197.
756 Cartwright, J., Santamarina, C., 2015. Seismic characteristics of fluid escape pipes in sedimentary
757 basins: Implications for pipe genesis. Marine and Petroleum Geology 65, 126–140.
758 Casas, D., Ercilla, G., Baraza, J., 2003. Acoustic evidences of gas in the continental slope sediments of
759 the Gulf of Cadiz (E Atlantic). Geo-Marine Letters 23, 300–310.
760 Cashman, K.V., Popenoe, P., 1985. Slumping and shallow faulting related to the presence of salt on the
761 continental slope and rise off North Carolina. Marine and Petroleum Geology 2, 260–271.
762 Doi.org/10.1016/0264-8172(85)90016-9.
763 Diez, S., Gràcia, E., Gutscher, M.A., Matias, L., Mulder, T., Terrinha, P., Somoza, L., 2005. Bathymetric
764 map of the Gulf of Cadiz, NE Atlantic Ocean: The SWIM multibeam compilation. Instrumentation
765 Viewpoint 4, 42–43.
766 Ehlers, J., Gibbard, P.L., 2007. The extent and chronology of Cenozoic Global Glaciation. Quaternary
767 International 164, 6–20.

Ercilla, G., Alonso, B., Wynn, R.B., Baraza, J., 2002. Turbidity current sediment waves on irregular slopes: observations from the Orinoco sediment-wave field. Marine Geology 192, 171–187.

Ercilla, G., Juan, C., Hernandez-Molina, F. J., Bruno, M., Estrada, F., Alonso, B., Casas, D., Farran, M., Llave, E., García, M., Vázquez, J.T. d'Acremont, E., Gorini, C., Palomino, D., Valencia, J., El Moumni, B., Ammar, A., 2016. Significance of bottom currents in deep-sea morphodynamics: an example from the Alboran Sea. Marine Geology 378, 157–170.

Ercilla, G., Juan, C., Periáñez, R., Alonso, B., Abril, J. M., Estrada, F., Casas, C., Vázquez, J.T., d'Acremont, E., Gorini, C, El Moumni, B., Do Couto, D., Valencia, J., 2019. Influence of alongslope processes on modern turbidite systems and canyons in the Alboran Sea (southwestern Mediterranean). Deep Sea Research Part I: Oceanographic Research Papers 144, 1–16.

Faugères, J.C., Gonthier, E., Stow, D.A.V., 1984. Contourite drift molded by deep Mediterranean outflow. Geology 12, 296–300.

Faugères, J.C., Mézerais, M.L., Stow, D.A.V., 1993a. Contourite drift types and their distribution in the North and South Atlantic Ocean basins. Sedimentary Geology 82, 189–203.

Faugères, J.C., Stow, D.A.V., 1993b. Bottom-current–controlled sedimentation: a synthesis of the contourite problem. Sedimentary Geology 82, 287–297.

Faugères, J.C., Stow, D.A.V., Imbert, P., Viana, A., 1999. Seismic features diagnostic of contourite drifts. Marine Geology 162, 1–38.

Faugères, J.C., Gonthier, E., Cirac, P., Castaing, P., Bellec, V., 2000a. Origine des dunes géantes rencontrées sur le plateau Landais (Golfe de Gascogne). VIIème Colloque International d'Océanographie du Golfe de Gascogne, Actes de Colloques, IFREMER 31, 26–31.

Faugères, J.C., Viana, A., Gonthier, E., Migeon, S., Stow, D.A.V., 2000b. Seismic features diagnostic of contourite drifts and sediment waves. In: Deep-Water Sedimentation: the Challenges for the Next Millennium, 31st IGC Workshop, Rio 2000, Deep-Seas, Abstr., pp. 26–32.

Fedele, J.J., García, M.H., 2009. Laboratory experiments on the formation of subaqueous depositional gullies by turbidity currents. Marine Geology 258, 48–59.

Fernández-Salas, L.M., Sánchez-Rubio, N., Vázquez, J.T., Díaz del Río, V., López-González, N., Sánchez-Leal, R., Bruque, G., López-Rodríguez., F.J., Palomino, D., Fernández-Puga, M., 2015. Geostatistical analysis of the submarine channels in the upper slope of the Gulf of Cadiz (SW Iberian Peninsula). Resúmenes sobre el VIII Simposio MIA15, Málaga.

Fernández-Puga, M.C., Vázquez, J.T., Somoza, L., Díaz del Río, V., Medialdea, T., Mata, M.P., León, R., 2007. Gas-related morphologies and diapirism in the Gulf of Cadiz. Geo-Marine Letters 27, 213–221.

Fernández-Puga, M.C., Vázquez, J.T., Medialdea, T., Somoza, L., Díaz del Río, V., León, R., 2010. Morphological and geophysical evidences of tectonic activity in the Gulf of Cadiz northern continental slope sector. Iberian Meeting on Active Faults and Palaeoseismology, Sigüenza, Spain. Abstract volume, 159–162.

Fernández-Puga, M.C., Vázquez, J.T., Sánchez-Guillamón, O., Pajarón, L., Fernández-Salas, L.M., Palomino, D., Díaz del Río, V., 2014. Evidences of contemporary tectonic activity along the Eastern Gulf of Cadiz continental shelf and upper slope. Iberfault, 2ª Reunión Ibérica sobre fallas activas y paleosismología, Abstract Volume 85–88.

Field, M.E., Gardner, J.V., Prior, D.B., 1999. Geometry and significance of stacked gullies on the northern California slope. Marine Geology 154, 271–286.

Fonnesu, M., Palermo, D., Galbiati, M., Marchesini, M., Bonamini, E., Bendias, D., 2020. A new world-class deep-water play-type, deposited by the syndepositional interaction of turbidity flows and

bottom currents: The giant Eocene Coral Field in northern Mozambique. Marine and Petroleum Geology 111, 179–201.
García, M., Hernández-Molina, F.J., Llave, E., Stow, D.A.V., León, R., Fernández-Puga, M.C., Díaz del Río, V., Somoza, L., 2009. Contourite erosive features caused by the Mediterranean Outflow Water in the Gulf of Cadiz: Quaternary tectonic and oceanographic implications. Marine Geology 257, 24–40.
García, M., Dowdeswell, J.A., Ercilla, G., Jakobsson, M., 2012. Recent glacially influenced sedimentary processes on the East Greenland continental slope and deep Greenland Basin. Quaternary Science Reviews 49, 64–81.
García, M., Hernández-Molina, F.J., Alonso, B., Vázquez, J.-T., Ercilla, G., Llave, E., Casas, D., 2016. Erosive sub-circular depressions on the Guadalquivir Bank (Gulf of Cadiz): Interaction between bottom current, mass-wasting and tectonic processes. Marine Geology 378, 5–19.
Gardner, J.V., Kidd, R.B., 1983. Sedimentary processes on the Iberian continental margin viewed by long-range side-scan sonar. Gulf of Cadiz. Oceanologica Acta 6, 245–254.
Gong, C., Wang, Y., Zhu, W., Li, W., Xu, Q., 2013. Upper Miocene to Quaternary unidirectionally migrating deep-water channels in the Pearl River Mouth Basin, northern South China Sea. The American Association of Petroleum Geologists Bulletin 97, 285–308.
Gong, C., Wang, Y., Rebesco, M., Salon, S., Steel, R.J., 2018. How do turbidity flows interact with contour currents in unidirectionally migrating deep-water channels? Geology 46, 551–554.
Gonthier, E.G., Faugeres, J.-C., Stow, D.A.V., 1984. Contourite facies of the Faro drift, Gulf of Cadiz. In: Stow, D.A.V., Piper, D.J.W. (Eds.), Fine-Grained Sediments: Deep-Water Processes and Facies, Geological Society of London, Special Publications 15, pp. 775– 797.
Gonthier, E., Faugères, J.C., Gervais, A., Ercilla, G., Alonso, B., Baraza, J., 2002. Quaternary sedimentation and origin of the Orinoco sediment-wave field on the Demerara continental rise (NE margin of South America). Marine Geology 192, 189–214.
Grundlingh, M.L., 1981. On the observation of a solitary event in the Mediterranean outflow west of Gibraltar. "Meteor" Forsch. Ergebn. 23, 3–46.
Gütscher, M.-A., Dominguez, S., Westbrook, G.K., Gente, P., Babonneau, N., Mulder, T., Gonthier, E., Bartolome, R., Luis, J., Rosas, F., Terrinha, P., The Delila and DelSis Scientific Teams, 2009. Tectonic shortening and gravitational spreading in the Gulf of Cadiz accretionary wedge: Observations from multi-beam bathymetry and seismic profiling. Marine and Petroleum Geology 26, 647–659.
Gütscher, M.-A., Dominguez, S., Westbrook, G.K., Le Roy, P., Rosas, F., Duarte, J.C., Terrinha, P., Miranda, J.M., Graindorge, D., Gailler, A., Sallares, V., Bartolomé, R., 2012. The Gibraltar subduction: A decade of new geophysical data. Tectonophysics 574-575, 72–91.
Hanquiez, V., Mulder, T., Toucanne, S., Lecroart, P., Bonnel, C., Marchès, E., Gonthier, E., 2010. The sandy channel-lobe depositional systems in the Gulf of Cadiz: Gravity processes forced by contour current processes. Sedimentary Geology 229, 110–123.
Hampton, M.A., Lee, H.J., Locat, J., 1996. Submarine landslides. Reviews of Geophysics 34, 33-59.
Haq,. B.U., Hardenbol, J., Vail, P.R., 1987. Chronology of fluctuating sea levels since the Triassic. Science 235, 1156–1167.
Hayward, B.W., Grenfell, H.R., Sabaa, A.T., Sikes, E.L., 2005. Deep-sea benthic foraminiferal record of the Middle Pleistocene Climate Transition in the South-west Pacific. In: M. J. Head and P. L. Gibbard (Eds.) Early Middle Pleistocene transitions: the land-ocean evidence. Geological Society (London), Special Publication 247, pp. 85–115
Head,M.J., Gibbard, P.L., 2005. Early–Middle Pleistocene Transitions: The Land–Ocean Evidence. Geological Society, London, Special Publications 247..

858 Hernández-Molina, F.J., Llave, E., Somoza, L., Fernandez-Puga, M., Maestro, A., Leon, R., Medialdea, T.,
859 Barnolas, A., García, M., del Rio, V., Fernandez-Salas, L., Vazquez, J., Lobo, F., Dias, J., Rodero, J. and
860 Gardner, J., 2003. Looking for clues to paleoceanographic imprints: A diagnosis of the Gulf of Cadiz
861 contourite depositional systems. Geology 31, 19–22.
862 Hernández-Molina, F.J., Llave, E., Stow, D.A.V., García, M., Somoza, L., Vazquez, J., Lobo, F., Maestro,
863 A., del Rio, V., Leon, R., Medialdea, T. and Gardner, J., 2006. The contourite depositional system of
864 the Gulf of Cadiz: A sedimentary model related to the bottom current activity of the Mediterranean
865 outflow water and its interaction with the continental margin. Deep-Sea Research Part II-Topical
866 Studies in Oceanography 53, 1420–1463.
867 Hernández-Molina, F.J., Llave, E., Preu, B., Ercilla, G., Fontan, A., Bruno, M., Serra, N., Gomiz, J.,
868 Brackenridge, R., Sierro, F., Stow, D.A.V., García, M., Juan, C., Sandoval, N., Arnaiz, A., 2014.
869 Contourite processes associated with the Mediterranean Outflow Water after its exit from the
870 Gibraltar Strait; global and conceptual implications. Geology 42, 231–234.
871 Hernández-Molina, F.J., Sierro, F.J., Llave, E., Roque, C., Stow, D.A.V., Williams, T., Lofi, J., Van der
872 Schee, M., Arnaiz, A., Ledesma, S., Rosales, C., Rodriguez-Tovar, F.J., Pardo-Iguzquiza, E. and
873 Brackenridge, R.E., 2016. Evolution of the Gulf of Cadiz margin and southwest Portugal contourite
874 depositional system: Tectonic, sedimentary and paleoceanographic implications from IODP
875 expedition 339. Marine Geology 337, 7–39.
876 Hovland, M., Judd, A.G., 1988. Seabed Pockmarks and Seepages: Geological Ecological and
877 Environmental Implication. Springer, 336 pp.
878 Howe, J.A., 1996. Turbidite and contourite sediment waves in the northern Rockall Trough, North
879 Atlantic Ocean, Sedimentology 43, 219–234.
880 Jackson, M.P.A., Hudec, M.R., 2017. Salt tectonics. Principles and practice. Cambridge University Press,
881 https://doi.org/10.1017/9781139003988.
882 Juan, C., Ercilla, G., Estrada, F., Alonso, B., Casas, D., Vázquez, J. T., d'Acremont, E., Medialdea, T.,
883 Hernández-Molina, F.J., Gorini, C., El Moumni, B., Valencia, J., 2020. Multiple factors controlling the
884 deep marine sedimentation of the Alboran Sea (SW Mediterranean) after the Zanclean Atlantic
885 Mega-flood. Marine Geology 423, 106138.
886 Kuvaas, B., Kristoffersen, Y., Leitchenkov, G., Guseva, J., Gandjukhin, V., 2004. Seismic expression of
887 glaciomarine deposits in the eastern Riiser Larsen Sea, Antarctica. Marine Geology 207, 1–15.
888 Lamb, K.G., 2014. Internal wave breaking and dissipation mechanisms on the continental slope/shelf.
889 Annual Review of Fluid Mechanics 46:231–54.
890 León, R., Somoza, L., Medialdea, T., Hernández-Molina, F.J., Vázquez, J.T., Díaz-del-Río, V., González,
891 F.J., 2010. Pockmarks, collapses and blind valleys in the Gulf of Cadiz. Geo-Marine Letter 30, 231–
892 247.
893 Li, H., Wang, Y., Zhu, W., Xu, Q., He, Y., Tang, W., Zhuo, H., Wang, D., Wu, J., Li, D., 2013. Seismic
894 characteristics and processes of the Plio-Quaternary unidirectionally migrating channels and
895 contourites in the northern slope of the South China Sea. Marine and Petroleum Geology 43, 370–
896 380.
897 Lisiecki, L.E., Raymo, M.E., 2005. A Pliocene-Pleistocene stack of 57 globally distributed benthic d18O
898 records. Paleoceanography 20, doi.org/10.1029/2004PA001071.
899 Locker, S.D., Laine, E.P., 1992. Paleogene-Neogene depositional history of the middle U.S. Atlantic
900 continental rise: mixed turbidite and contourite depositional systems. Marine Geology 103, 137–
901 164.

902 Llave, E., Hernández-Molina, F.J., Somoza, L., Díaz-del-Río, V., Stow, D.A.V., Maestro, A., Alveirinho
903 Dias, J.M., 2001. Seismic stacking pattern of the Faro-Albufeira contourite system (Gulf of Cadiz): A
904 Quaternary record of paleoceanographic and tectonic influences. Marine Geophysical Researches
905 22, 487–508.
906 Llave, E., Schonfeld, J., Hernández-Molina, F.J., Mulder, T., Somoza, L., Díaz del Rio, V. and Sanchez-
907 Almazo, I., 2006. High-resolution stratigraphy of the Mediterranean outflow contourite system in
908 the Gulf of Cadiz during the late Pleistocene: The impact of Heinrich events. Marine Geology 227,
909 241–262.
910 Llave, E., Hernández-Molina, F.J., Somoza, L., Stow, D.A.V., Díaz del Río, V., 2007a. Quaternary
911 evolution of the contourite depositional system in the gulf of Cadiz. In: Viana, A., Rebesco, M.
912 (Eds.), Economic and Paleoceanographic Importance of Contourites. Geological Society of London
913 Special Publication 276, pp. 49–79.
914 Llave, E., Hernández-Molina, F.J., Stow, D.A.V., Fernández-Puga, M.C., García, M., Vázquez, J.T.,
915 Maestro, A., Somoza, L., Díaz del Río, V., 2007b. Reconstructions of the Mediterranean Outflow
916 Water during the quaternary based on the study of changes in buried mounded drift stacking
917 pattern in the Gulf of Cadiz. Marine Geophysical Researches 28, 379–394.
918 Llave, E., Matias, H., Hernández-Molina, F.J., Ercilla, G., Stow, D.A.V., Medialdea, T., 2011. Pliocene and
919 Quaternary seismic stacking pattern and distribution of contourites in the Algarve margin (Northern
920 Gulf of Cadiz, Spain). Geo-Marine Letters 31, 377–390.
921 Llave, E., Hernández-Molina, F.J., García, M., de Weger, W., Ng, Z.L., Duarte, D., de Castro, S., Sierro,
922 F.J., Navas, J., 2019. Distribution of the Southern Contourite Channel (SE Gulf of Cadiz) since the
923 opening of the Strait of Gibraltar. 58th BSRG, London. Abstracts Volume.
924 Locker, S.D., Laine, E.P., 1992. Paleogene-Neogene depositional history of the middle U.S. Atlantic
925 Continental Rise; Mixed turbidite and contourite depositional systems. Marine Geology 103, 137–
926 164.
927 Lofi, J., Voelker, A.H.L., Ducassou, E., Hernández-Molina, F.J., Sierro, F.J., Bahr, A., Galvani, A., Lourens,
928 L.J., Pardo-Igúzquiza, E., Rodríguez-Tovar, F.J., William, T., 2016. Quaternary record in the gulf of
929 Cadiz and Portuguese contourite depositional systems. Marine Geology 377, 40–57.
930 Lozano, P. et al., 2020. Multiprocess interaction shaping geoforms and controlling substrate types and
931 benthic community distribution in the Gulf of Cadiz. Marine Geology 423, 106139.
932 Louarn, E., Morin, P., 2011. Antarctic Intermediate Water influence on Mediterranean Sea Water
933 outflow. Deep Sea Research Part I: Oceanographic Research Papers 58, 932–942.
934 Lopes, F.C., Cunha, P.P., Le Gall, B., 2006. Cenozoic seismic stratigraphy and tectonic evolution of the
935 Algarve margin (offshore Portugal, southwestern Iberian Peninsula). Marine Geology 231, 1-36.
936 Mack, G.H., 1978. The survivability of labile light mineral grains in fluvial, aeolian and littoral marine
937 environments: The Permian Cutler and Cedar Mesa Formation, Moab, Utah. Sedimentology 25,
938 587–606.
939 Madelain, F., 1970. Influence de la topographie du fond sur l'ecoulement méditerranéen entre le
940 Detroit de Gibraltar et le Cap Saint-Vincent. Cahiers Océanographiques 22, 43–61.
941 Maestro, A., Somoza, L., Medialdea, T., Talbot, C.J., Lowrie, A., Vázquez, J.T., Díaz-del-Río, V., 2003.
942 Large-scale slope failure involving Triassic and Middle Miocene salt and shale in the Gulf of Cadiz
943 (Atlantic Iberian Margin). Terra Nova 15, 380–391.
944 Maestrelli, D., Iacopini, D., Jihad, A.A., Bond, C.E., Bonini, M,. 2017. Seismic and structural
945 characterization of fluid escape pipes using 3D and partial stack seismic from the Loyal Field

946 (Scotland, UK): A multiphase and repeated intrusive mechanism. Marine and Petroleum Geology
947 88, 489-510.
948 Maldonado, A., Somoza, L., Pallares, L., 1999. The Betic orogen and the Iberian-African boundary in the
949 Gulf of Cadiz: geological evolution (central North Atlantic). Marine Geology 155, 9–43.
950 Marchès, E., Mulder, T., Cremer, M., Bonnel, C., Hanquiez, V., Gonthier, E., Lecroart, P., 2007.
951 Contourite drift construction influenced by capture of Mediterranean Outflow Water deep-sea
952 current by the Portimao submarine canyon (Gulf of Cadiz, South Portugal). Marine Geology 242,
953 247–260.
954 Marchès, E., Mulder, T., Gonthier, E., Cremer, M., Hanquiez, V., Garlan, T., Lecroart, P., 2010. Perched
955 lobe formation in the Gulf of Cadiz: Interactions between gravity processes and contour currents
956 (Algarve Margin, Southern Portugal). Sedimentary Geology 229, 81–94.
957 Martínez-Loriente, S., Sallarès, V., Gràcia, E., Bartolome, R., Dañobeitia, J., Zitellini, N., 2014. Seismic
958 and gravity constraints on the nature. Journal of Geophysical Research: Solid Earth 119, 127–149.
959 Martorelli, E., Bosman, A., Casalbore, D., Falcini, F., 2016. Interaction of down-slope and along-slope
960 processes off Capo Vaticano (Southern Tyrrhenian Sea, Italy), with particular reference to
961 contourite-related landslides. Marine Geology 378, 43–55.
962 Maselli, V., Kneller, B., 2018. Bottom currents, submarine mass failures and halokinesis at the toe of
963 the Sigsbee Escarpment (Gulf of Mexico): contrasting regimes during lowstand and highstand
964 conditions? Marine Geology 401, 36–65.
965 Masson, D.G., Howe, J.A., Stoker, M.S., 2002. Bottom-current sediment waves, sediment drifts and
966 contourites in the northern Rockall Trough. Marine Geology 192, 215–237.
967 McAdoo, B.G., Pratson, L.F., Orange, D.L., 2000. Submarine landslide geomorphology, US continental
968 slope. Marine Geology 169, 103–136.
969 Medialdea, T., Vegas, R., Somoza, L., Vázquez, J.T., Maldonado, A., Díaz-del-Río, V., Maestro, A.,
970 Córdoba, D., Fernández-Puga, M.C., 2004. Structure and evolution of the “Olistostrome” complex of
971 the Gibraltar Arc in the Gulf of Cadiz (eastern Central Atlantic): evidence from two long seismic
972 cross-sections. Marine Geology 209, 173–198.
973 Medialdea, T., Somoza, L., Pinheiro, L., Fernandez-Puga, M., Vazquez, J., Leon, R., Ivanov, M.,
974 Magalhaes, V., Diaz-del-Rio, V. and Vegas, R., 2009. Tectonics and mud volcano development in the
975 Gulf of Cadiz. Marine Geology 261, 48–63.
976 Mestdagh, T., Lobo, F.J., Llave, E., Hernández-Molina, F.J., Van Rooij, D., 2019. Review of the late
977 Quaternary stratigraphy of the northern Gulf of Cadiz continental margin: New insighs into
978 controlling factors and global implications. Earth-Science Reviews 198,
979 doi:10.1016/j.earscirev.2019.102944.
980 Micallef, A., Mountjoy, J.J., Barnes, P.M., Canals, M., Lastras, G., 2014. Geomorphic response of
981 submarine canyons to tectonic activity: Insights from the Cook Strait canyon system, New Zealand.
982 Geosphere 10, 905–929.
983 Michels, K.H., Kuhn, G., Hillenbrand, C.-D., Diekmann, B., Fütterer, D.K., Grobe, H., Uenzelmann-Neben,
984 G., 2002. The southern Weddell Sea: combined contourite-turbidite sedimentation at the
985 southeastern margin of the Weddell Gyre, in: Stow, D.A.V., Pudsey, C.J., Howe, J.A., Faugères, J.-C.,
986 Viana, A.R. (Eds.), Deep-Water Contourite Systems: Modern Drifts and Ancient Series, Seismic and
987 Sedimentary Characteristics. Geological Society, London, Memoirs, 22, pp. 305–323.
988 Miramontes, E., Penven, P., Fierens, R., Droz, L., Toucanne, S., Jorry, S.J., Jouet, G., Pastor, L., Silva
989 Jacinto, R., Gaillot, A., Giraudeau, J., Raisson, F., 2019. The influence of bottom currents on the

990 Zambezi Valley morphology (Mozambique Channel, SW Indian Ocean): In situ current observations
991 and hydrodynamic modelling. Marine Geology 410, 42–55.
992 Miramontes, E., Eggenhuisen, J.T., Silva Jacinto, R., Poneti, G., Pohl, F., Normandeau, A., Campbell,
993 D.C., Hernández-Molina, F.J., 2020. Channel-levee evolution in combined contour current-turbidity
994 current flows from flume-tank experiments. Geology 48, doi.org/10.1130/G47111.1.
995 Mountjoy, J.J., Barnes, P.M., Pettinga, J.R., 2009, Morphostructure and evolution of submarine
996 canyons across an active margin: Cook Strait sector of the Hikurangi Margin, New Zealand: Marine
997 Geology 260, 45–68.
998 Mulder, T., Cochonat, P., 1996. Classification of offshore mass movements. Journal of Sedimentary
999 Research 66, 43–57.
1000 Mulder, T., Faugères, J.C., Gonthier, E., 2008. Mixed Turbidite–Contourite Systems, in: Rebesco, M.,
1001 Camerlenghi, A. (Eds.), Contourites. Developments in Sedimentology. Elsevier, Amsterdam, 60, pp.
1002 435–456.
1003 Mulder, T., Lecroart, P., Hanquiez, V., Marches, E., Gonthier, E., Guedes, J.-C., Thiébot, E., Jaaidi, B.,
1004 Kenyon, N., Voisset, M., Pérez, C., Sayago, M., Fuchey, Y., Bujan, S., 2006. The western part of the
1005 Gulf of Cadiz: contour currents and turbidity currents interactions. Geo-Marine Letters 26, 31–41.
1006 Mulder, T., Gonthier, E., Lecroart, P., Hanquiez, V., Marchès, E., Voisset, M., 2009. Sediment failures
1007 and flows in the Gulf of Cadiz (eastern Atlantic). Marine and Petroleum Geology 26, 660–672.
1008 Nelson, C.H., Baraza, J. Maldonaldo, A., 1993. Mediterranean Undercurrent Sandy Contourites, Gulf of
1009 Cadiz, Spain. Sedimentary Geology 82, 103–131.
1010 Nelson, C.H., Baraza, J., Maldonado, A., Rodero, J., Escutia, C.,Barber Jr., J.H., 1999. Influence of the
1011 Atlantic inflow and Mediterranean outflow currents on Late Quaternary sedimentary facies of the
1012 Gulf of Cadiz continental margin. Marine Geology 155, 99–129.
1013 Nelson, C.H., Maldonado, A., 1988., Factors controlling depositional patterns of Ebro turbidite
1014 systems, Mediterranean Sea. American Association of Petroleum Geologists Bulletin, 72, 698–716.
1015 Ochoa, J., Bray, N.A., 1991. Water mass exchange in the Gulf of Cadiz. Deep-Sea Research 38, S465–
1016 S503.
1017 Palomino, D., López-González., N., Vázquez, J.-T., Fernández-Salas, L.-M., Rueda, J.L., Sánchez-Leal, R.,
1018 Díaz-del-Río, V., 2016. Multidisciplinary study of mud volcanoes and diapirs and their relationship to
1019 seepages and bottom currents in the Gulf of Cadiz continental slope (northeastern sector). Marine
1020 Geology 378, 196–212.
1021 Pellegrini, C., Maselli, V., Trincardi, F., 2016. Pliocene–Quaternary contourite depositional system along
1022 the south-western Adriatic margin: changes in sedimentary stacking pattern and associated bottom
1023 currents. Geo-Marine Letters 36, 67–70.
1024 Piper, D.J.W., Mosher, D.C., Campbell, D.C., 2012. Controls on the distribution of major types of
1025 submarine landslides. In: Clague, J.J. and Stead, D. (Eds.), Landslides: types, mechanisms, and
1026 modeling. Cambridge University Press, pp. 95–107.
1027 Platt, J.P., Allerton, S., Kirker, A., Mandeville, C., Mayfield, A., Platzman, E.S., Rimi, A., 2003. The
1028 ultimate arc: differential displacement, oroclinal bending, and vertical axis rotation in the External
1029 Betic-Rif arc. Tectonics 22, 1017, doi:10.1029/2001TC001321.
1030 Platt, J.P., Behr, W.M., Johanesen, K., Williams, J.R., 2013. The Betic-Rif Arc and its orogenic hinterland:
1031 a review. Annual Review of Earth and Planetary Sciences 41, 313–357.
1032 Plaza-Faverola, A., Bünz, S., Mienert, J., 2011. Repeated fluid expulsion through sub-seabed chimneys
1033 offshore Norway in response to glacial cycles. Earth and Planetary Science Letters 305, 297-308).

1034 Posamentier, H.W., Martinsen, O.J., 2010. The character and genesis of submarine mass-transport
1035 deposits: insights from outcrop and 3D seismic data. SEPM Special Publications 95, 7–38.
1036 Rasmussen, S., Lykke-Andersen, H., Kuijpers, A., Troelstra, S.R., 2003. Post-Miocene sedimentation at
1037 the continental rise of Southeast Greenland: the interplay between turbidity and contour currents.
1038 Marine Geology 196, 37–52.
1039 Rebesco, M., Pudsey, C.J., Canals, M., Camerlenghi, A., Barker, P.F., Estrada, F., Giorgetti, A., 2002.
1040 Sediment drifts and deep-sea channel systems, Antarctic Peninsula Pacific Margin, in: Stow, D.A.V.,
1041 Pudsey, C.J., Howe, J.A., Faugères, J.-C., Viana, A.R. (Eds.), Deep-Water Contourite Systems: Modern
1042 Drifts and Ancient Series, Seismic and Sedimentary Characteristics. Geological Society, London,
1043 Memoirs, 22, pp. 353–371.
1044 Rebesco, M., Hernádez-Molina, F.J., Van Rooij, D., Wåhlin, A., 2014. Contourites and associated
1045 sediments controlled by deep-water circulation processes: State-of-the-art and future
1046 considerations. Marine Geology 352, 111–154.
1047 Richards, M., Bowman, M. and Reading, H. 1998. Submarine-fans systems I: Characterization and
1048 stratigraphic prediction. Marine and Petroleum Geology 15, 689–717.
1049 Rinke-Hardekopft, L., Reuning, L., Bourget, J., Back, S., 2018. Syn-sedimentary deformation as a
1050 mechanism for the initiation of submarine gullies on a carbonate platform to slope transition,
1051 Browse Basin, Australian North West Shelf. Marine and Petroleum 91, 622–630.
1052 Rodero, J., Pallarés, L., Maldonado, A., 1999. Late Quaternary seismic facies of the Gulf of Cadiz
1053 Spanish margin: depositional processes influenced by sea-level change and tectonic controls.
1054 Marine Geology 155, 131–156.
1055 Rodríguez, K., Hodgson, N., 2019. Hydrocarbon potential of hybrid depositional systems. GEOExPro 16,
1056 44–46.
1057 Roque, C., Duarte, H., Terrinha, P., Valadares, V., Noiva, J., Cahão, M., Ferreira, J., Legoínha, P., Zitellini,
1058 N., 2012. Pliocene and Quaternary depositional model of the Algarve margin contourite drifts (Gulf
1059 of Cadiz, SW Iberia): seismic architecture, tectonic control and paleoceanographic insights. Marine
1060 Geology 303–306, 42–62.
1061 Roque, D., Parras-Berrocal, I., Bruno, M., Sánchez-Leal., R., Hernández-Molina, F.J., 2019. Seasonal
1062 variability of intermediate water masses in the Gulf of Cadiz: implications of the Antarctic and
1063 subarctic seesaw. Ocean Science 15, 1–17.
1064 Rosenbaum, G., Lister, G.,Duboz, C., 2002. Reconstruction of the tectonic evolution of the western
1065 Mediterranean since the Oligocene. Journal of the Virtual Explorer 8, 107–130.
1066 Ruano, P., Bohoyo, F., Galindo-Zaldívar, J., Pérez, L.F., Hernández-Molina, F.J., Maldonado, A., García,
1067 M., Medialdea, T., 2014. Mass transport processes in the Southern Scotia Sea: evidence of
1068 paleoearthquakes. Global and Planetary Change 123, 374-391.
1069 Ryan, W. B. F., Carbotte, S.M., Coplan, J., O'Hara, S., Melkonian, A., Arko, R., Weissel, R.A., Ferrini, V.,
1070 Goodwillie, A., Nitsche, F., Bonczkowski, J., Zemsky, R., 2009. Global Multi-Resolution Topography
1071 (GMRT) synthesis data set. Geochemistry, Geophysics. Geosystems 10, Q03014,
1072 doi:10.1029/2008GC002332.
1073 Sánchez-Leal, R.F., Bellanco, M.J., Fernández-Salas, L.M., García-Lafuente, J., Gasser-Rubinat, M.,
1074 González-Pola, C., Hernández-Molina, F.J., Pelegrí, J.L., Peliz, A., Relvas, P., Roque, D., Ruiz-Villarreal,
1075 M., Sammartino, S., Sánchez-Garrido, J.C., 2017. The Mediterranean Overflow in the Gulf of Cadiz: A
1076 rugged journey. Science Advances 3:eaao0609.
1077 Sánchez-Rubio, N., Fernández-Salas, L.M., Vázquez, J.T., Díaz del Río, V., López-González, N., Sánchez-
1078 Leal., R., Bruque, G., López-Rodríguez., F.J., Palomino, D., Fernández-Puga, M.C., 2015.

1079 Morphological characterization of submarine channels in the upper slope of the Gulf of Cadiz (SW
1080 Iberian Peninsula). Resúmenes sobre el VIII Simposio MIA15, Málaga.
1081 Sansom, P., 2018. Hybrid turbidite–contourite systems of the Tanzanian margin. Petroleum Geoscience
1082 24, 258–276.
1083 Schattner, U., Lobo, F.J., García, M., Kanari, M., Ramos, R.B., de Mahiques, M.M., 2018. A detailed look
1084 at diapir piercement onto the ocean floor: New evidence from Santos Basin, offshore Brazil. Marine
1085 Geology 406, 98–108.
1086 Serra, C.S., Martínez-Loriente, S., Gràcia, E., Urgeles, R., Vizcaino, A., Perea, H., Bartolome, R., Pallàs,
1087 R., Lo Iacono, C., Diez, S., Dañobeitia, J., Terrinha, P., Zitellini, N., 2020. Tectonic evolution,
1088 geomorphology and influence of bottom currents along a large submarine canyon system: The São
1089 Vicente Canyon (SW Iberian margin). Marine Geology 426, doi: 10.1016/j.margeo.2020.106219.
1090 Serra, N., Ambar, I., Käse, R., 2005. Numerical modelling of the Mediterranean Water splitting and
1091 eddy generation, Deep-Sea Research I 52, 383–408.
1092 Serra, N., Ambar, I., Boutov, D., 2010. Surface expression of Mediterranean Water dipoles and their
1093 contribution to the shelf/slope – open ocean exchange. Ocean Science 6, 191–209.
1094 Shanmugam, G., 2007. The obsolescence of deep-water sequence stratigraphy in petroleum geology.
1095 Indian Journal of Petroleum Geology 16, 1–45.
1096 Shanmugam, G., 2012. New Perspectives on Deep-Water Sandstones: Origin, Recognition, Initiation,
1097 and Reservoir Quality. Elsevier, Oxford, 544 pp.
1098 Somoza, L., Diaz-del-Rio, V., Leon, R., Ivanov, M., Fernandez-Puga, M., Gardner, J., Hernández-Molina,
1099 F.J., Pinheiro, L., Rodero, J., Lobato, A., Maestro, A., Vazquez, J., Medialdea, T. and Fernandez-Salas,
1100 L., 2003. Seabed morphology and hydrocarbon seepage in the Gulf of Cadiz mud volcano area:
1101 Acoustic imagery, multibeam and ultra-high resolution seismic data. Marine Geology 195, 153–176.
1102 Somoza, L., Lowrie A., Maestro, A., 1999. Allochtonous Blocks as Hydrocarbon Traps in the Gulf of
1103 Cadiz. Offshore Technology Conference 31, Vol. 1, 571–577.
1104 Spinelli, G., Field, M.E., 2001. Evolution of continental slope gullies on the Northern California. Journal
1105 of Sedimentary Research 71, 237–245.
1106 Teixeira, M., Terrinha P., Roque C., Rosa M., Ercilla G., Casas D, 2019. Interaction of alongslope and
1107 downslope processes in the Alentejo Margin (SW Iberia) - Implications on slope stability. Marine
1108 Geology 410, 88–108.
1109 Terrinha, P., Ribeiro, C., Kullberg, J.C., Rocha, R., Ribeiro, A., 2002. Compression episodes during rifting
1110 and faunal isolation in the Algarve Basins, SW Iberia. Journal of Geology 110, 101–113.
1111 Terrinha, P., Matias, L., Vicente, J., Duarte, J., Pinhero, L., Lourenço, N., Diez, S., Rosas, F., Magalhaes,
1112 V., Valadares, V., Zitellini, N., Roque, C., Mendes Víctor, L., MATESPRO Team, 2009.
1113 Morphotectonics and strain partitioning at the Iberia-Africa plate boundary from multibeam and
1114 seismic reflection data. Marine Geology 267, 165–174.
1115 Thorpe, S.A., 1976. Variability of the Mediterranean undercurrent in the Gulf of Cadiz. Deep-Sea
1116 Research 23, 711–727.
1117 Torelli, L., Sartori, R., Zitellini, N., 1997.The giant chaotic body in the Atlantic ocean off Gi-braltar: new
1118 results from a deep seismic reflection survey. Marine and Petroleum Geology 14, 125–138.
1119 Toucanne, S., Mulder, T., Schönfeld, J., Hanquiez, V., Gonthier, E., Duprat, J., Cremer, M., Zaragosi, S.,
1120 2007. Contourites of the Gulf of Cadiz: A high-resolution record of the paleocirculation of the
1121 Mediterranean outflow water during the last 50,000 years. Palaeogeography, Palaeoclimatology,
1122 Palaeoecology 246, 354–336.

Tripsanas, E.K., Bryant, W.R., Prior, D.B., Phaneuf, B.A., 2003. Interplay Between Salt Activities and Slope Instabilities, Bryant Canyon Area, Northwest Gulf of Mexico, in: Locat, J., Mienert, J., Boisvert, L. (Eds.), Submarine Mass Movements and Their Consequences: 1st International Symposium. Springer Netherlands, Dordrecht, pp. 307–315.

Tripsanas, E.K., Bryant, W.R., Phaneuf, B.A., 2004. Slope-instability processes caused by salt movements in a complex deep-water environment, Bryant Canyon area, northwest Gulf of Mexico. The American Association of Petroleum Geologists Bulletin 88, 801–823.

Tsai, C.-H., Huang, C.-L., Hsu, S.-K., Doo, W.-B., Lin, S.-S., Wang, S.-Y., Lin, J.-Y., Liang, C.-W., 2018. Active normal faults and submarine landslides in the Keelung Shelf off NE Taiwan. Terrestrial, Atmospheric and Oceanic Sciences 29, 31–38.

Twichell, D.C., Chaytor, J.D., ten Brink, U.S., Buczkowski, B., 2009. Morphology of late Quaternary landslides along the U.S. Atlantic continental margin. Marine Geology 264, 4–15.

Van Rooij, D., Iglesias, J., Hernández-Molina, F.J., Ercilla, G., Gomez-Ballesteros, M., Casas, d., Llave, E., De Hauwere, A., Garcia-Gil, S., Acosta, J., Henriet, J.-P., 2010. The Le Danois Contourite Depositional System: Interactions between the Mediterranean Outflow Water and the upper Cantabrian slope (North Iberian margin). Marine Geology 274, 1–20.

Vargas, C.A., Mann, P., Gómez, C., 2012. Morphologic expression of accretionary processes and recent submarine landslides along the Southwestern Pacific Margin of Colombia. In: Yamada, Y., Kawamura, K., Ikehara, K., Ogawa, Y., Urgeles, R., Mosher, D., Chaytor, J., Strasser, M. (Eds.), Submarine Mass Movements and Their Consequences. Springer, Netherlands, pp. 365–377.

Vázquez, J.-T., López-González., N., Fernández-Salas, L., Díaz del Río, V., Fernández-Puga, M.C., Palomino, D., Mata, M.P., Bárcenas, P., Sayago-Gil., M., Bruque, G., 2010. Nuevos datos de actividad tectónica durante el Pleistoceno Superior-Holoceno en el sector oriental de la plataforma continental del Golfo de Cadiz (SO de Iberia). In: Insúa, J.M., Martín-González, F. (Eds.), Contribución de la Geología al Análisis de la Peligrosidad Sísmica. DOI: 10.13140/2.1.3265.0245.

Viana, A.R., 2009. Economic Relevance of Contourites. In: Rebesco, M., Camerlenghi, A. (Eds.), Contourites. Developments in Sedimentology, pp. 493–510.

Wynn, R.B., Stow, D.A.V., 2002. Classification and characterisation of deep-water sediment waves. Marine Geology 192, 7–22.

Youbin, H., Zhengzhong, G., Jinxiong, L., Shunshe, L., Xuefeng, L., 2008. Characteristics of internal-wave and internal-tide deposits and their hydrocarbon potential. Petroleum Science 5, 37–44.

Zenk, W. ,1975. On the Mediterranean outflow west of Gibraltar. Meteor Forschungsergeb 16, 23–34.

Figure Captions

Figure 1. a) Regional bathymetric map of the Gulf of Cadiz contourite depositional system showing the main MOW cores and branches. ML: Mediterranean Lower core; MU: Mediterranean Upper core; SB: Southern branch; PB: Principal branch; IB: Intermediate branch; 1: proximal scour and sand ribbons sector; 2: active contourite drift sector; CC: Contourite channel; SD: Sheeted drift; GDR: Guadalquivir diapiric ridge; CDR: Cadiz diapiric ridge; b) Datasets used in this work include the swath bathymetric mosaic and airgun and multichannel seismic lines.

Figure 2. a) Flow distribution of the MOW along the upper and middle slope. Flow direction and velocity is taken from Sánchez-Leal et al. (2017); CC; Contourite channel; b) Hydrographic profiles showing the distribution of the East North Antarctic Central Water (ENACW) and the Mediterranean Outflow Water (MOW) that affect at present day the Cadiz upper and middle slope (modified from Sánchez-Leal et al., 2017).

Figure 3. a) Bathymetric map of the study area showing the location of the correlated profiles in b) and c); CC: Contourite Channel (N: Northern; S: Southern; T: Tofiño; G: Gusano; H: Huelva; C: Cadiz); CDR: Cadiz diapiric ridge; GDR: Guadalquivir diapiric ridge; b) airgun line CADIZ21; c) multichannel line S81A-16, modified from Hernández-Molina et al. (2014, 2016), from which the Mid-Pleistocene Discontinuity (MPD) and Late Quaternary Discontinuity (LQD) have been taken. d) Table showing the links between the seismic units and sub-units from this work with previous stratigraphic units and discontinuities. The units and sub-units are tentatively correlated with the climatic record represented by the benthic d18O isotopic curve of Lisiecki and Raymo (2005).

Figure 4. Physiographic characterization of the Gulf of Cadiz continental margin close to the Strait of Gibraltar. a) Bathymetric map showing the physiographic domains, the location of the study area and the three major areas (Southern, Central and Northern) considered in this work; b) Bathymetric profiles from the outer continental shelf down to the proximal middle slope. See location in a and b).

Figure 5. a) Bathymetry of the continental margin showing the location of the study area and the bathymetry and profiles shown in Fig.5b to Fig.5e; b) 3D model of the study area showing the Southern, Central and Northern areas considered in this work; c) Detail of the bathymetric map showing sediment waves; c) Detail of the bathymetric map showing the sediment waves in the Northern area; d) shelf-edge escarpment and its bathymetric profile; e) Topographic profiles across the slope gullies.

Figure 6. a) Map of the basement depth, showing the main features that include two NE-SW-oriented depressions and small basins. Outcropping diapirs are shown in orange colors, and white dots represent the top of buried diapirs. This figure shows the two main orientations of these aligned diapirs, NW-SE and NE-SW; CC: Contourite Channel; CDR: Cadiz diapiric ridge; GDR: Guadalquivir diapiric ridge; b) Multichannel seismic profiles showing the basement, diapirs and faults in a downslope direction.

Figure 7. Shallower airgun profiles in orientations parallel to the isobaths and their interpretation. The seismic units and sub-units and their seismic character is detailed, as well as the features identified in the profiles (faults, gullies, chaotic-transparent deposits). The alignment of diapir

tops are shown. Orange: NE-SW-oriented diapirs. Blue: NW-SW-oriented diapirs. CDR: Cadiz diapiric ridge; GDR: Guadalquivir diapiric ridge.

Figure 8. Deeper airgun profiles in orientations parallel to the isobaths and their interpretation. The seismic units and sub-units and their seismic character is detailed, as well as the features identified in the profiles (faults, gullies, chaotic-transparent deposits). The alignment of diapir tops are shown. Orange: NE-SW-oriented diapirs. Blue: NW-SW-oriented diapirs. CDR: Cadiz diapiric ridge; GDR: Guadalquivir diapiric ridge.

Figure 9. a) Bathymetric map showing the location of the airgun profiles shown in Fig. 9b, Fig. 10 and Fig. 11 and the position of buried and outcropping diapirs. Orange: NE-SW-oriented diapirs. Blue: NW-SW-oriented diapirs; b) Airgun profile and stratigraphic interpretation orientated perpendicular to the isobaths in the Southern area. The seismic units and sub-units and their seismic character is detailed, as well as the features identified in the profiles. See location and legends in a).

Figure 10. Airgun profile and stratigraphic interpretation orientated perpendicular to the isobaths in the Central area. The seismic units and sub-units and their seismic character is detailed, as well as the features identified in the profiles. The mounded-prograding deposits in sub-unit Q6-c is detailed in the zoomed image. See location and legends in Fig. 9a.

Figure 11. Airgun profile and stratigraphic interpretation orientated perpendicular to the isobaths in the Northern area. The seismic units and sub-units and their seismic character is detailed, as well as the features identified in the profiles. See location and legends in Fig. 9a; HCC: Huelva contourite channel.

Figure 12. Isochore maps highlighting the distribution of depocenters of the two main seismic units and topography of their base (MPD: Mid Pleistocene Discontinuity; LQD; Late Quaternary Discontinuity) and isochore maps of the sub-units depocenters. CDR: Cadiz diapiric ridge; GDR: Guadalquivir diapiric ridge. The present-day location of the shelf break (discontinuous dark blue line) and main contourite channels (CC, in pink) along the middle slope is included as a reference.

Figure 13. Sketches of the diapiric activity, bottom current distribution and sedimentary processes along the two stages of evolution of the Gulf of Cadiz continental margin in the area close to the Strait of Gibraltar: a) Mid Pleistocene Discontinuity to Late Quaternary Discontinuity; b) Late Quaternary Discontinuity to Present. The base topography of the base of unit Q5 (MPD) and Q6 (LQD) are shown for reference.

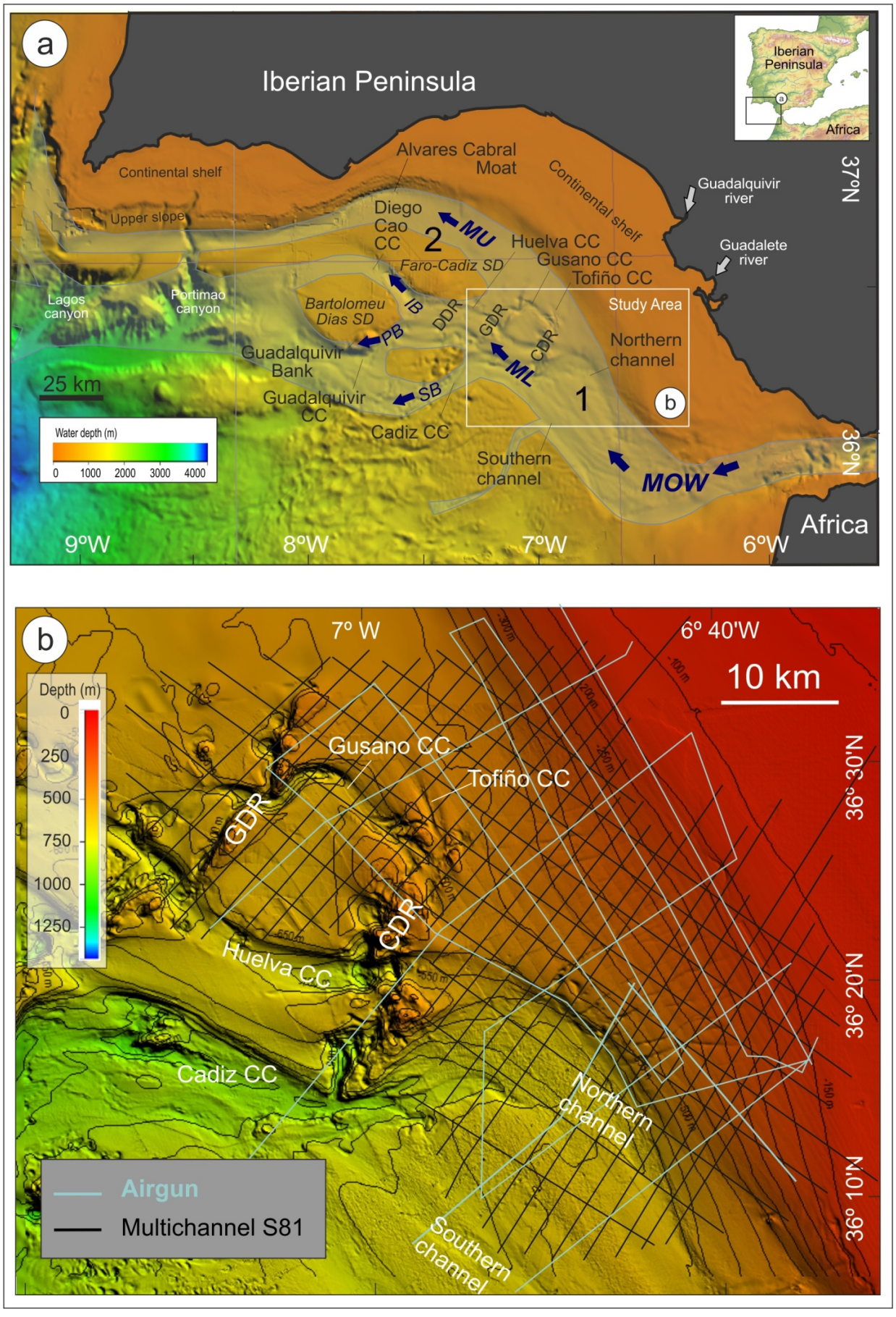
a
Iberian Peninsula
Iberian Peninsula
Africa
Alvares Cabral Moat
Continental shelf
Upper slope
Continental shelf
Guadalquivir river
Guadalete river
37ºN
Diego Cao CC
2
MU
Huelva CC
Gusano CC
Tofiño CC
Faro-Cadiz SD
Lagos canyon
Portimao canyon
Bartolomeu Dias SD
IB
DDR
GDR
CDR
Study Area
Northern channel
PB
Guadalquivir Bank
ML
1
b
25 km
Guadalquivir CC
SB
Cadiz CC
Water depth (m)
0 1000 2000 3000 4000
Southern channel
MOW
36ºN
Africa
9ºW
8ºW
7ºW
6ºW
b
7º W
6º 40'W
10 km
Depth (m)
0
250
500
750
1000
1250
Gusano CC
Tofiño CC
GDR
CDR
Huelva CC
Cadiz CC
Northern channel
Southern channel
Airgun
Multichannel S81
36º 30'N
36º 20'N
36º 10'N

1228

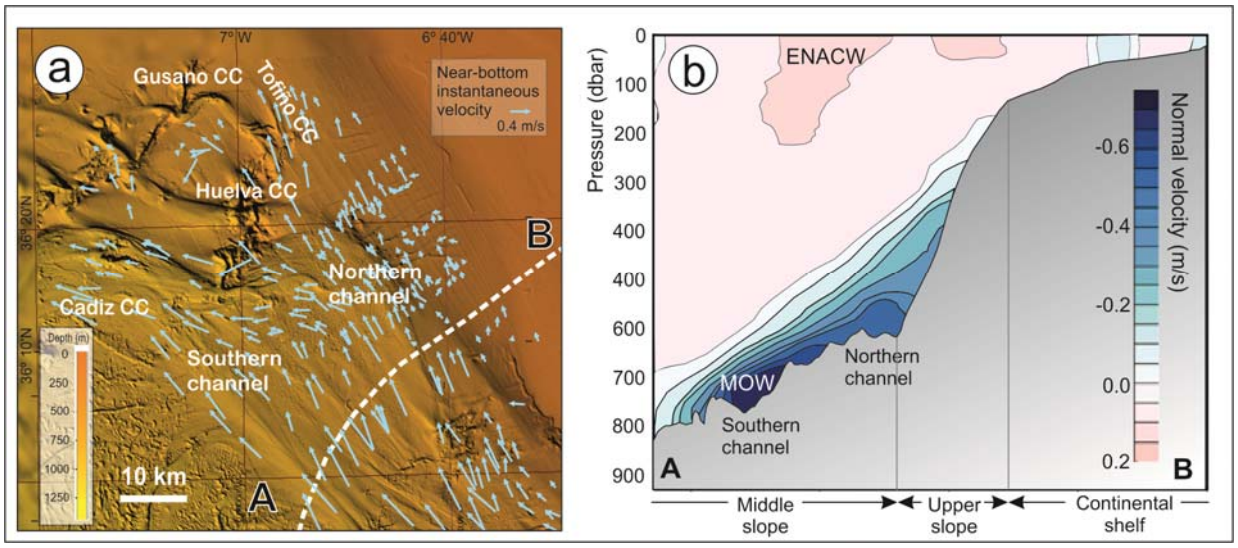
a
7° W
6° 40'W
36° 20'N
36° 10'N
Gusano CC
Tomino CC
Huelva CC
Cadiz CC
Northern channel
Southern channel
Near-bottom instantaneous velocity
0.4 m/s
Depth (m)
0
250
500
750
1000
1250
10 km
A
B
b
ENACW
MOW
Northern channel
Southern channel
Pressure (dbar)
0
100
200
300
400
400
600
700
800
900
Normal velocity (m/s)
-0.6
-0.4
-0.2
0.0
0.2
A
B
Middle slope
Upper slope
Continental shelf

1229

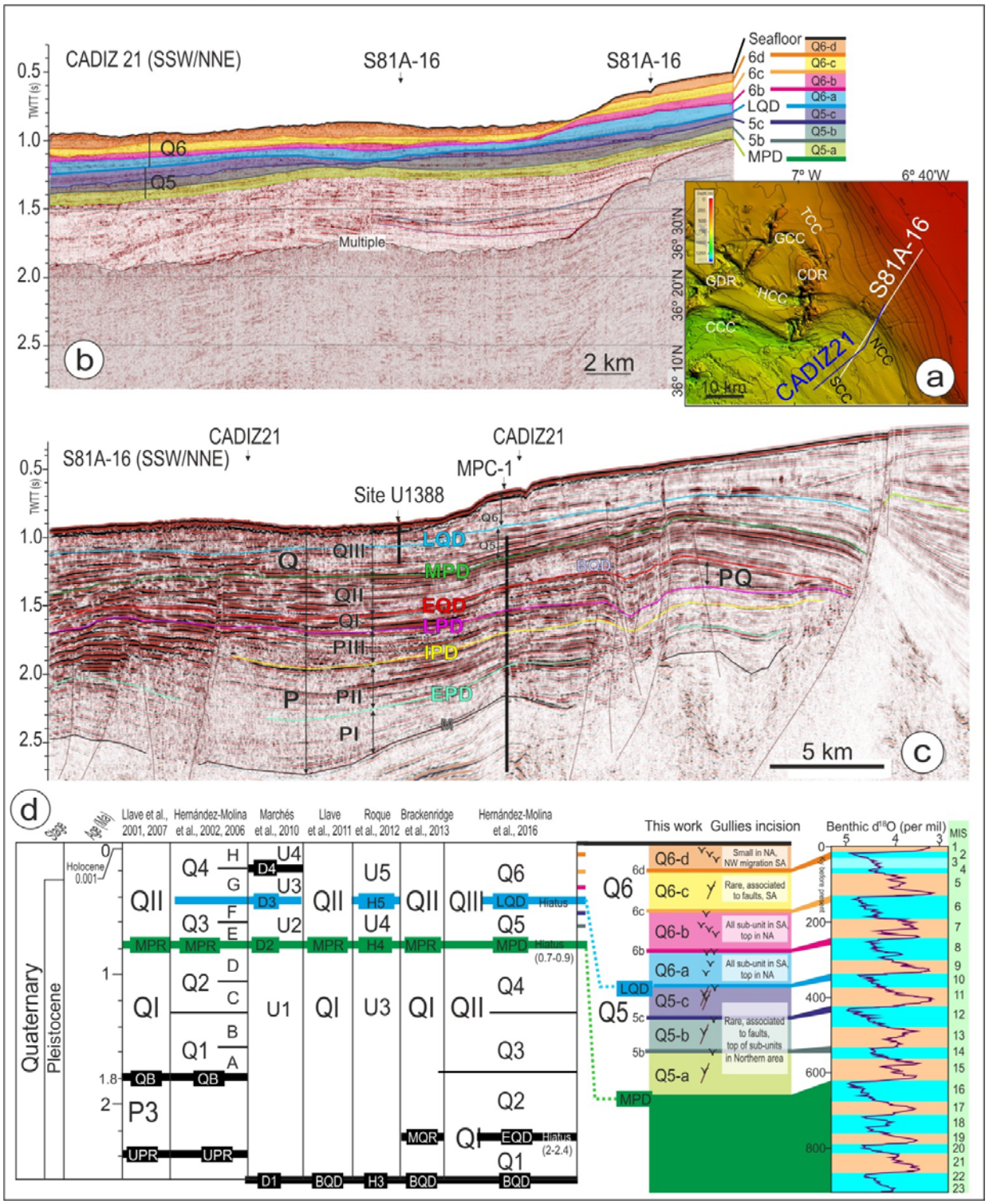
CADIZ 21 (SSW/NNE)
S81A-16
S81A-16
Seafloor
6d
6c
6b
LQD
5c
5b
MPD
Q6-d
Q6-c
Q6-b
Q6-a
Q5-c
Q5-b
Q5-a
TWTT (s)
Q6
Q5
Multiple
2 km
b
7° W
6° 40'W
36° 30'N
36° 20'N
36° 10'N
TCC
GCC
CDR
CDR
HCC
CCC
S81A-16
CADIZ21
NCC
SCC
10 km
a
S81A-16 (SSW/NNE)
CADIZ21
MPC-1
CADIZ21
Site U1388
Q6
Q5
LQD
MPD
EQD
LPD
IPD
EPD
BQD
Q
QIII
QII
QI
PIII
P
PII
PI
M
PQ
5 km
c
d
Llave et al., 2001, 2007
Hernández-Molina et al., 2002, 2006
Marchés et al., 2010
Llave et al., 2011
Roque et al., 2012
Brackenridge et al., 2013
Hernández-Molina et al., 2016
Quaternary
Pleistocene
Holocene
0.001
QII
QI
P3
MPR
QB
UPR
Q4
Q3
Q2
Q1
U4
U3
U2
U1
D4
D3
D2
D1
H5
H4
H3
QII
QI
QIII
LQD
MPD
EQD
MQR
BQD
Hiatus
(0.7-0.9)
(2-2.4)
Q6
Q5
Q4
Q3
Q2
Q1
This work Gullies incision
Q6-d
Q6-c
Q6-b
Q6-a
Q5-c
Q5-b
Q5-a
Small in NA, NW migration SA
Rare, associated to faults, SA
All sub-unit in SA, top in NA
All sub-unit in SA, top in NA
Rare, associated to faults, top of sub-units in Northern area
Benthic d18O (per mil)
MIS

1230

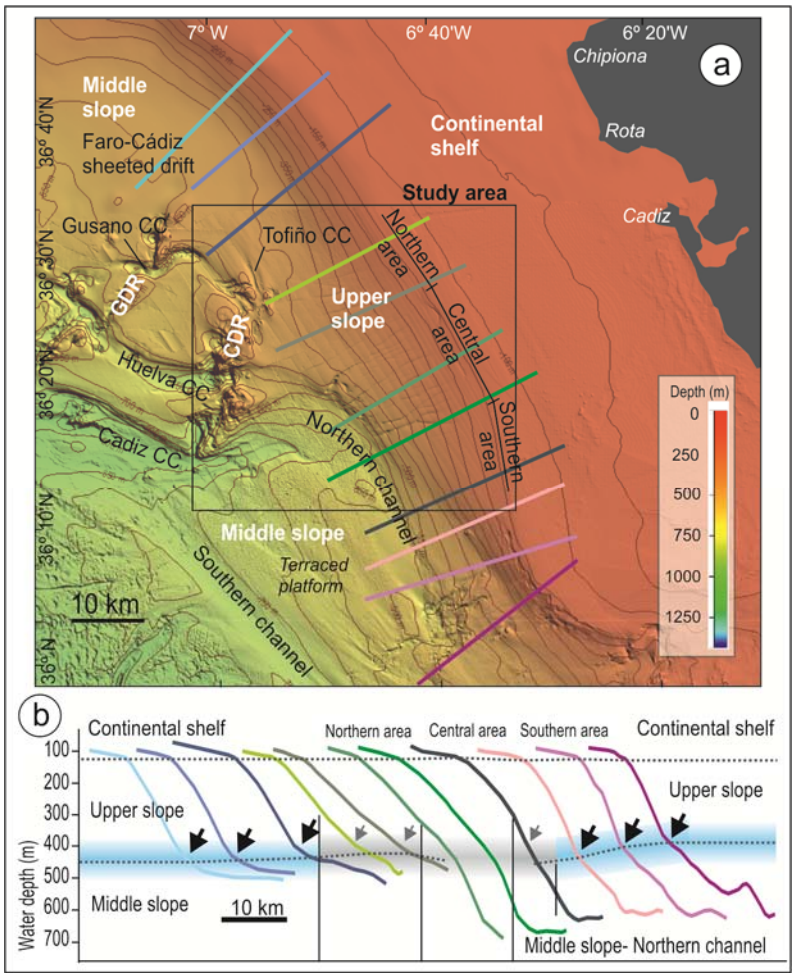
7° W
6° 40'W
6° 20'W
Chipiona
a
Middle slope
Faro-Cádiz sheeted drift
Continental shelf
Rota
Study area
Cadiz
36° 40'N
36° 30'N
36° 20'N
36° 10'N
36° N
Gusano CC
Tofiño CC
Northern area
Central area
Southern area
Upper slope
CDR
CDR
Huelva CC
Cadiz CC
Northern channel
Depth (m)
0
250
500
750
1000
1250
Middle slope
Terraced platform
Southern channel
10 km
b
Continental shelf
Northern area
Central area
Southern area
Continental shelf
Upper slope
Upper slope
Water depth (m)
100
200
300
400
500
600
700
Middle slope
10 km
Middle slope- Northern channel

1231

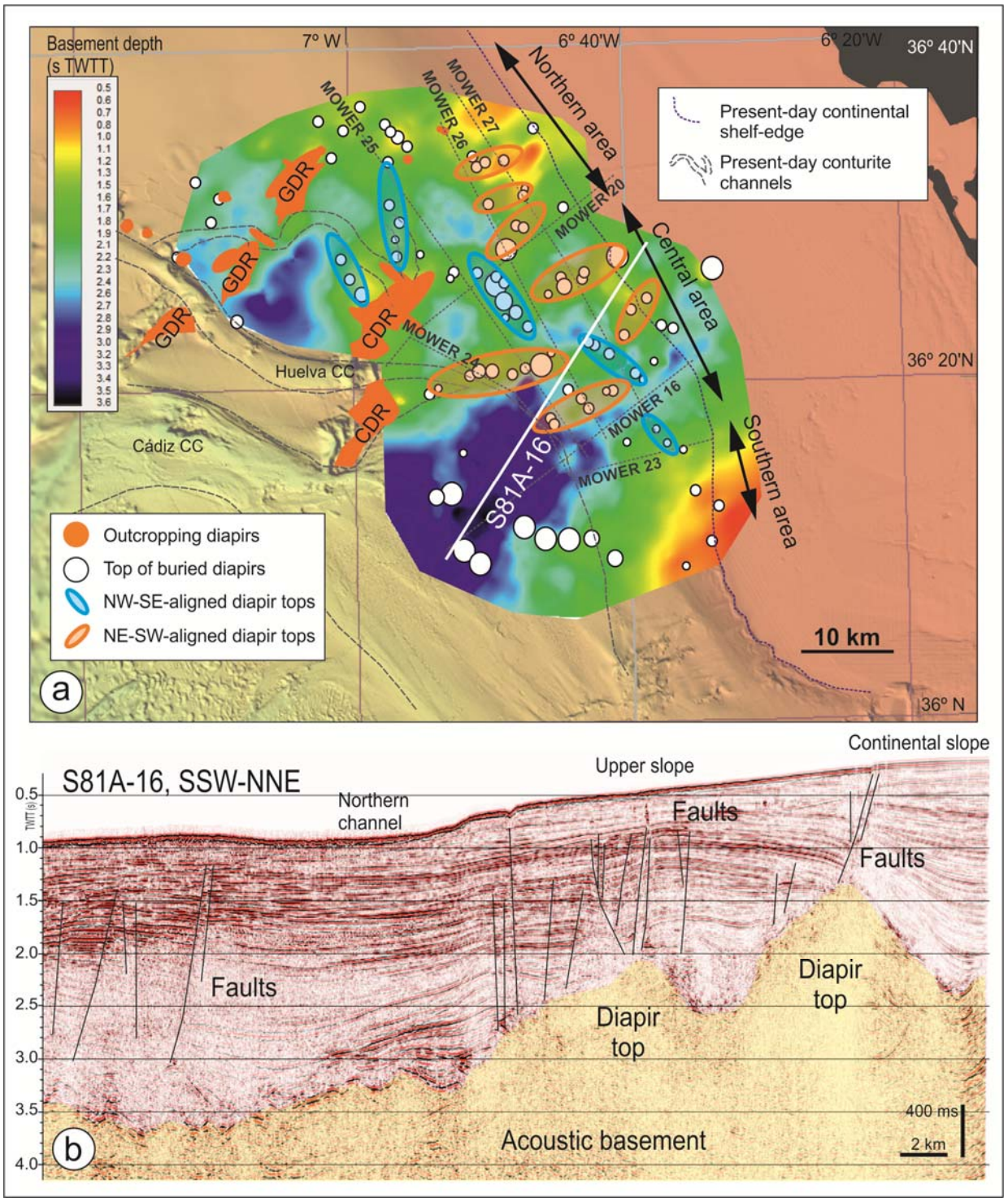
Basement depth
(s TWTT)
0.5
0.6
0.7
0.8
1.0
1.1
1.2
1.3
1.5
1.6
1.7
1.8
1.9
2.1
2.2
2.3
2.4
2.6
2.7
2.8
2.9
3.0
3.2
3.3
3.4
3.5
3.6
7° W
6° 40'W
6° 20'W
36° 40'N
36° 20'N
36° N
Present-day continental shelf-edge
Present-day conturite channels
Northern area
Central area
Southern area
MOWER 25
MOWER 27
MOWER 26
MOWER 20
MOWER 24
MOWER 16
MOWER 23
GDR
CDR
Huelva CC
Cádiz CC
S81A-16
Outcropping diapirs
Top of buried diapirs
NW-SE-aligned diapir tops
NE-SW-aligned diapir tops
10 km
a
S81A-16, SSW-NNE
Continental slope
Upper slope
Northern channel
Faults
Faults
Faults
Diapir top
Diapir top
Acoustic basement
TWTT (s)
0.5
1.0
1.5
2.0
2.5
3.0
3.5
4.0
400 ms
2 km
b

1232

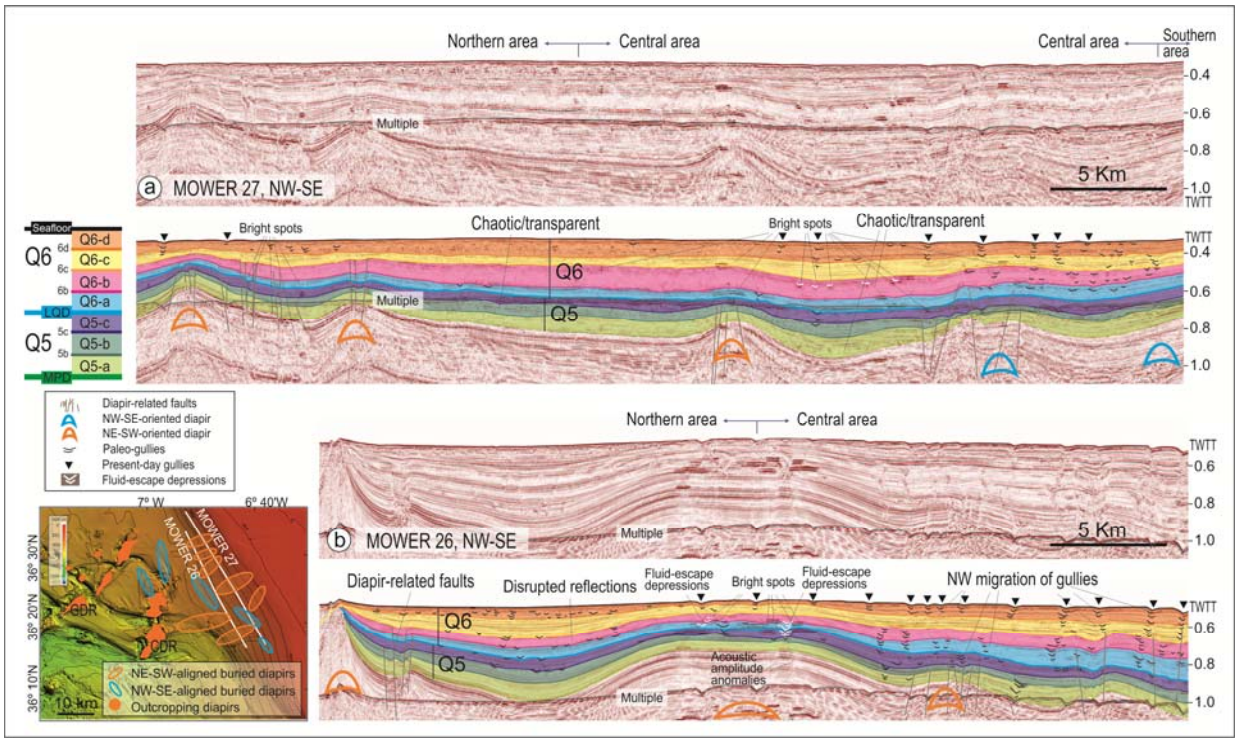
Northern area
Central area
Central area
Southern area
Multiple
a MOWER 27, NW-SE
5 Km
TWTT
0.4
0.6
0.8
1.0
Seafloor
Q6
Q6-d
Q6-c
Q6-b
Q6-a
LQD
Q5
Q5-c
Q5-b
Q5-a
MPD
Bright spots
Chaotic/transparent
Bright spots
Chaotic/transparent
Q6
Q5
Multiple
Diapir-related faults
NW-SE-oriented diapir
NE-SW-oriented diapir
Paleo-gullies
Present-day gullies
Fluid-escape depressions
7° W
6° 40'W
36° 30'N
36° 20'N
36° 10'N
MOWER 27
MOWER 26
GDR
GDR
NE-SW-aligned buried diapirs
NW-SE-aligned buried diapirs
Outcropping diapirs
10 km
Northern area
Central area
b MOWER 26, NW-SE
Multiple
5 Km
Diapir-related faults
Disrupted reflections
Fluid-escape depressions
Bright spots
Fluid-escape depressions
NW migration of gullies
Q6
Q5
Acoustic amplitude anomalies
Multiple

1233

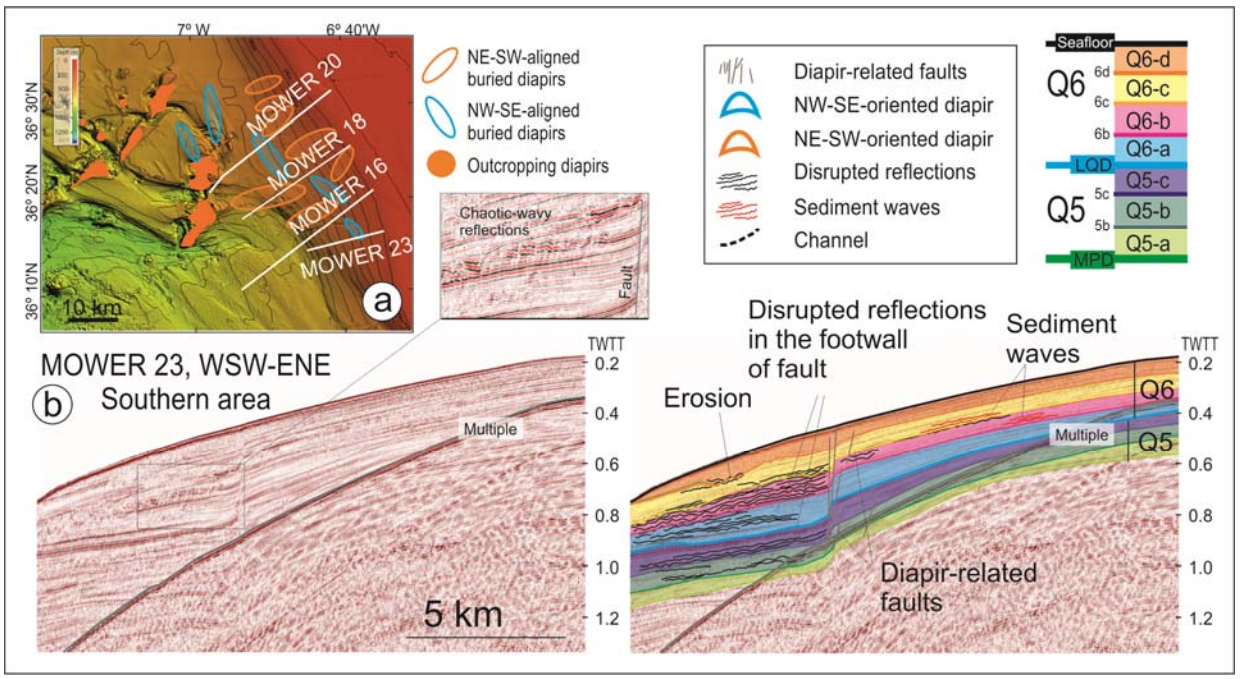
7° W
6° 40'W
36° 30'N
36° 20'N
36° 10'N
MOWER 20
MOWER 18
MOWER 16
MOWER 23
10 km
a
NE-SW-aligned buried diapirs
NW-SE-aligned buried diapirs
Outcropping diapirs
Chaotic-wavy reflections
Fault
Diapir-related faults
NW-SE-oriented diapir
NE-SW-oriented diapir
Disrupted reflections
Sediment waves
Channel
Seafloor
Q6
Q6-d
Q6-c
Q6-b
Q6-a
LQD
Q5
Q5-c
Q5-b
Q5-a
MPD
MOWER 23, WSW-ENE
b Southern area
Multiple
5 km
TWTT
0.2
0.4
0.6
0.8
1.0
1.2
Disrupted reflections in the footwall of fault
Sediment waves
Erosion
Q6
Q5
Multiple
Diapir-related faults

1234

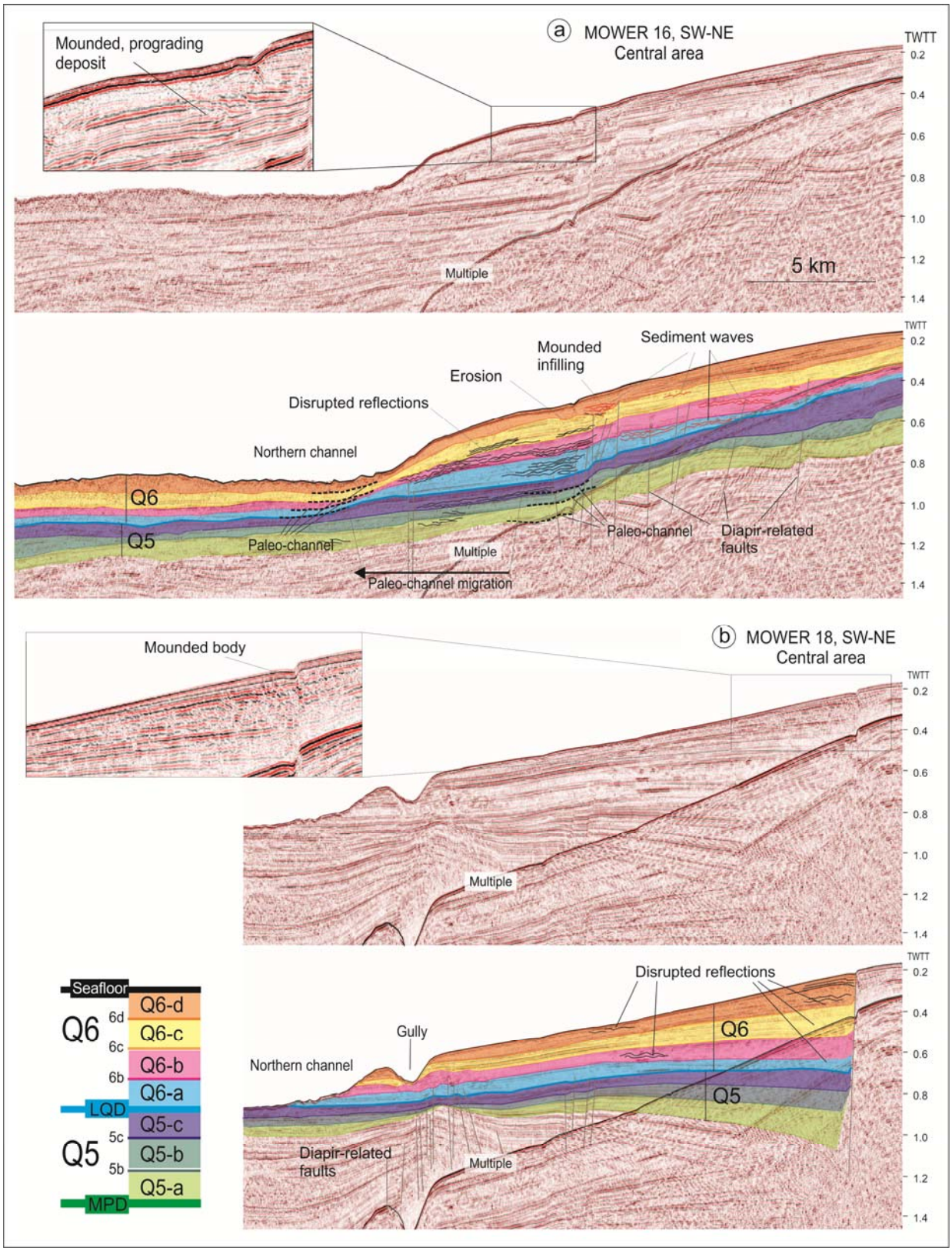
a MOWER 16, SW-NE
Central area
Mounded, prograding deposit
TWTT
0.2
0.4
0.6
0.8
1.0
1.2
1.4
Multiple
5 km
Sediment waves
Mounded infilling
Erosion
Disrupted reflections
Northern channel
Q6
Q5
Paleo-channel
Multiple
Paleo-channel migration
Paleo-channel
Diapir-related faults
b MOWER 18, SW-NE
Central area
Mounded body
Multiple
Seafloor
Q6
6d
Q6-d
6c
Q6-c
6b
Q6-b
Q6-a
LQD
Q5
5c
Q5-c
5b
Q5-b
Q5-a
MPD
Disrupted reflections
Gully
Q6
Northern channel
Q5
Diapir-related faults
Multiple

1235

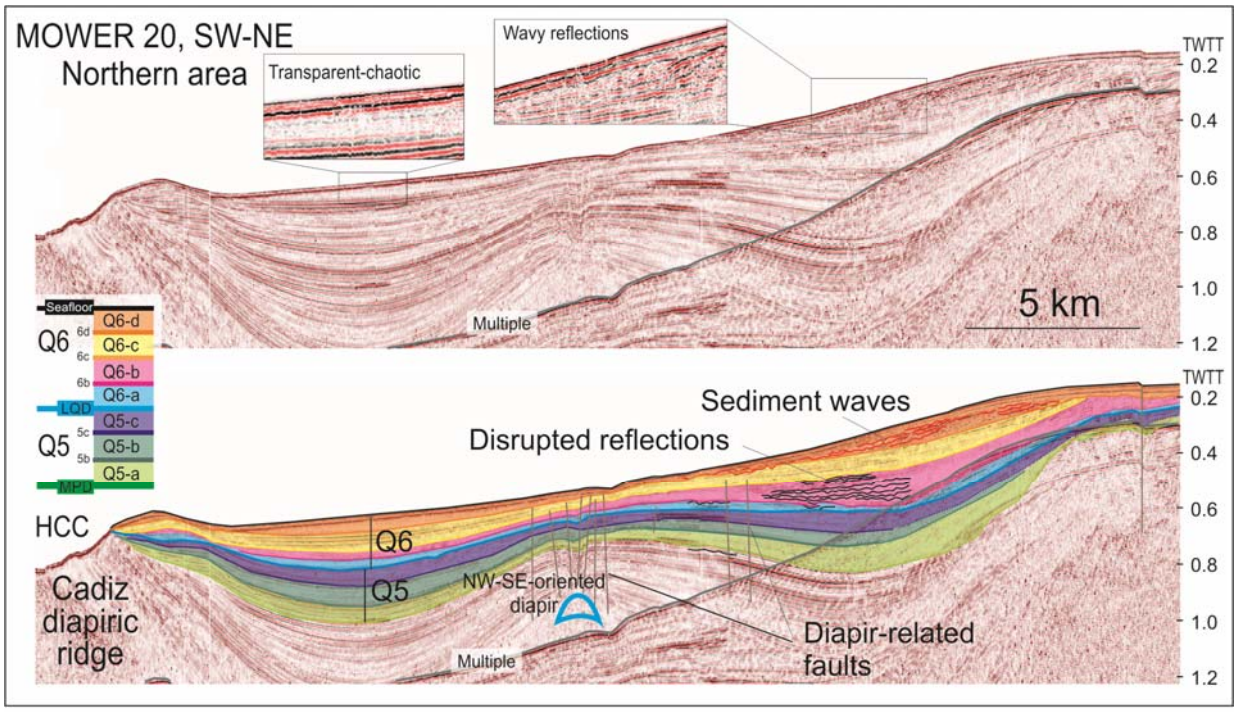
MOWER 20, SW-NE
Northern area
Transparent-chaotic
Wavy reflections
TWTT
0.2
0.4
0.6
0.8
1.0
1.2
5 km
Multiple
Seafloor
Q6
6d
Q6-d
6c
Q6-c
6b
Q6-b
Q6-a
LQD
Q5
5c
Q5-c
5b
Q5-b
Q5-a
MPD
Sediment waves
Disrupted reflections
HCC
Q6
Q5
Cadiz
diapiric
ridge
NW-SE-oriented
diapir
Diapir-related
faults
Multiple

1236

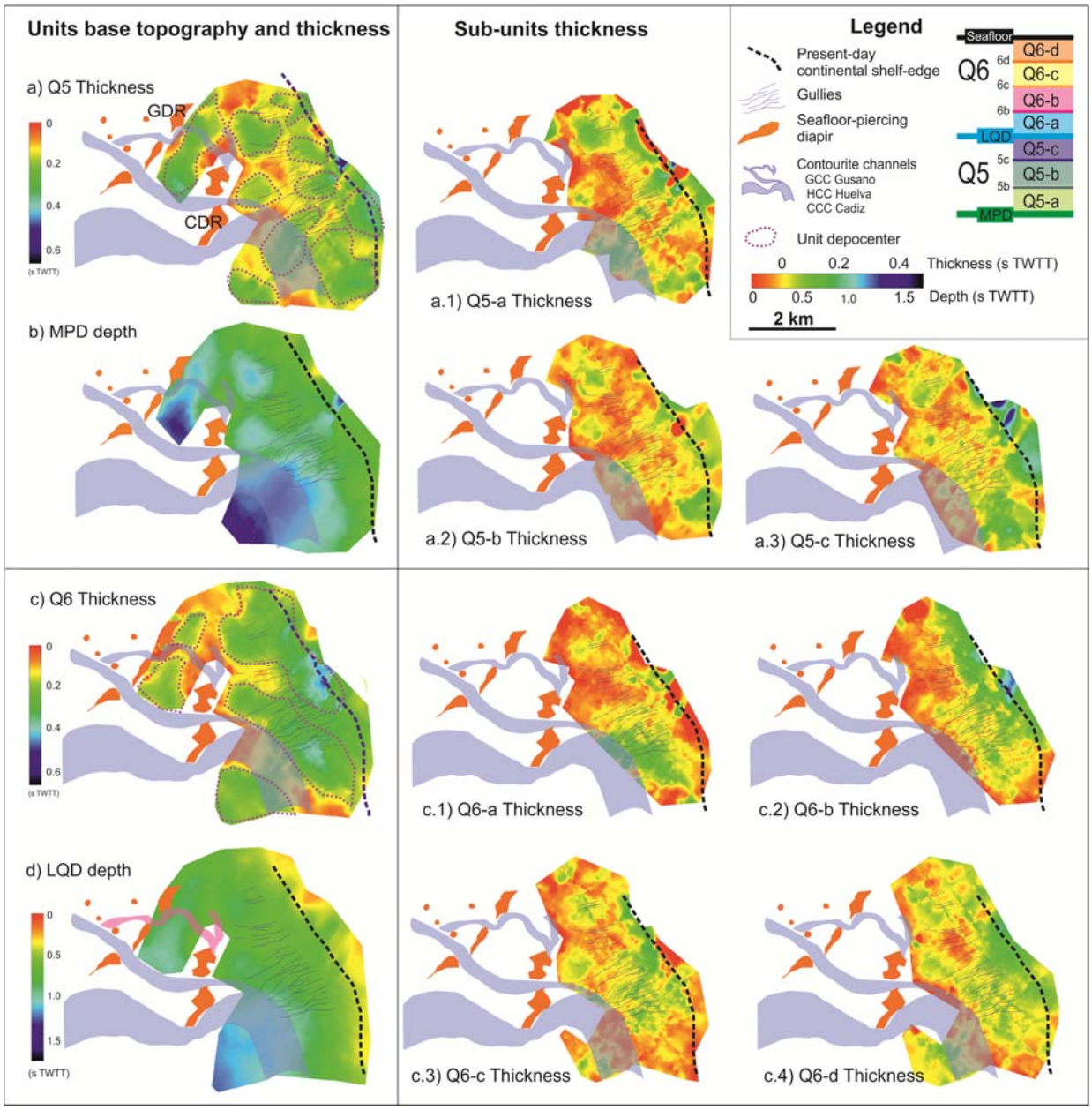
Units base topography and thickness
Sub-units thickness
Legend
a) Q5 Thickness
GDR
CDR
0
0.2
0.4
0.6
(s TWTT)
b) MPD depth
a.1) Q5-a Thickness
a.2) Q5-b Thickness
a.3) Q5-c Thickness
Present-day continental shelf-edge
Gullies
Seafloor-piercing diapir
Contourite channels
GCC Gusano
HCC Huelva
CCC Cadiz
Unit depocenter
Seafloor
Q6
6d
6c
6b
LQD
Q5
5c
5b
MPD
Q6-d
Q6-c
Q6-b
Q6-a
Q5-c
Q5-b
Q5-a
0 0.2 0.4 Thickness (s TWTT)
0 0.5 1.0 1.5 Depth (s TWTT)
2 km
c) Q6 Thickness
c.1) Q6-a Thickness
c.2) Q6-b Thickness
d) LQD depth
0
0.5
1.0
1.5
(s TWTT)
c.3) Q6-c Thickness
c.4) Q6-d Thickness

1237

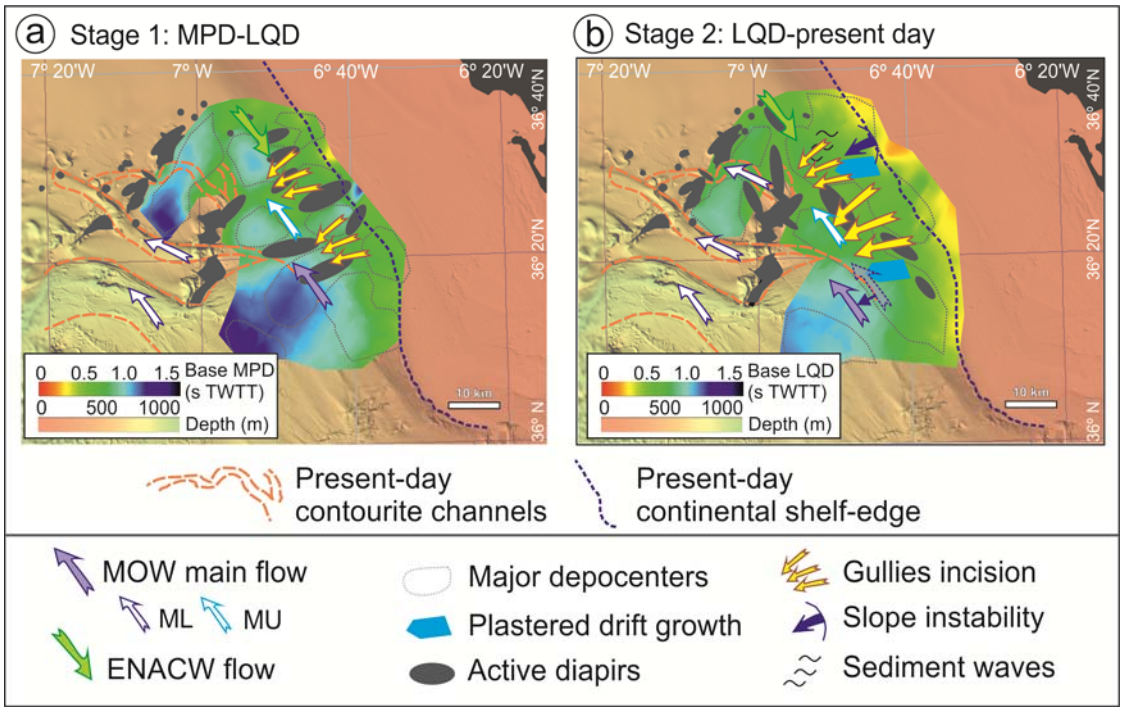
a Stage 1: MPD-LQD
b Stage 2: LQD-present day
7° 20'W
7° W
6° 40'W
6° 20'W
36° 40'N
36° 20'N
36° N
0 0.5 1.0 1.5 Base MPD (s TWTT)
0 500 1000 Depth (m)
0 0.5 1.0 1.5 Base LQD (s TWTT)
0 500 1000 Depth (m)
10 km
Present-day contourite channels
Present-day continental shelf-edge
MOW main flow
ML
MU
ENACW flow
Major depocenters
Plastered drift growth
Active diapirs
Gullies incision
Slope instability
Sediment waves

1238